JOURNAL OF MATERIALS SCIENCE 26 (1991) 1705–1728

Fabrication and characterization of thin films with perpendicular magnetic anisotropy for high-density magnetic recording

Part I *A review*

C. W. CHEN
Chemistry and Materials Science Department, Lawrence Livermore National Laboratory, University of California, Livermore, California 94550, USA

Perpendicular magnetic anisotropy (PMA) was first observed in thin films of cobalt–chromium alloys in 1974, and perpendicular magnetic recording was proposed in 1977. After less than ten years, a new technology for high-density magnetic recording is firmly established. This breakthrough of the science and technology of magnetic recording has been made possible mainly through the ingenuity and concerted efforts of researchers. The preparation, characterization, and application of the Co–Cr films featuring PMA have been extensively studied. This paper reviews the large number of reports on PMA films with emphasis on three areas: 1. processing of PMA films; 2. correlation of magnetic properties and microstructures of PMA films; and 3. state-of-art techniques for fabricating PMA films.

Nomenclature

PMA	Perpendicular magnetic anisotropy
PMR	Perpendicular magnetic recording
B	Magnetic induction
H	Magnetic field
H_c	Coercivity
$H_{c,\perp}$	Perpendicular coercivity
H_d	Demagnetizing field
H_K	Anisotropy field
$H_\perp$	Perpendicular anisotropy constant
M_r	Remanent magnetization
M_s	Saturation magnetization
P_{Ar}	Argon pressure
T_s	Substrate temperature
V_b	Substrate bias voltage
α	Incidence angle
$\Delta\theta_{50}$	Half-width dispersion angle in the rocking curve
θ_c	Curie temperature
σ_0	Internal stress

1. Introduction

Although the technology of magnetic information has been a mature industry for three decades, it has recently undergone dynamic evolutionary changes [1]. The changes came about partly because conventional storage media and recording heads cannot store information at the needed higher densities nor retrieve and transfer it at the necessary higher speeds. Also, there have been successful developments of thin-film media and heads featuring perpendicular magnetic anisotropy (PMA). Not only can the PMA films of the Co–Cr alloys be conveniently fabricated into storage media and recording heads, the new media and heads can store information at bit densities that are 2–3 orders of magnitude greater than that previously possible.

The possibility of using PMA films for high-density magnetic recording was first suggested by Iwasaki in 1975 [2]. Two years later, he formally proposed the perpendicular magnetic recording (PMR) technology, for which thin films of the Co–Cr alloy are the recommended fabrication material [3]. His proposal and the potential of this new approach to magnetic recording have greatly inspired researchers to work on PMA films and the PMR process. The rapid development of both vividly reflect the dynamic nature of magnetic-information technology.

As might be expected, the development of PMR technology has generated a voluminous literature. Although most papers about PMA films are informative and stimulating, some are redundant and inconsistent. This review deals with the major studies of the materials science of PMA films.

The review begins with the analytical work on the magnetization characteristics of PMA films (Section 2.1) and select analyses on PMR (Section 2.2). The choices of the alloy systems for PMA films are discussed in Section 3. Section 4 is concerned with the various methods for the fabrication of PMA films, Section 5 with the structural, magnetic, and corrosion and wear properties of Co–Cr films. The layered structures of PMA films for improved PMR performance are described in Section 6. Finally, Section 7 depicts the potential and future of PMR as described

0022–2461/91 $03.00 + .12 © 1991 Chapman and Hall Ltd.

by Iwasaki and others and the reviewer's own observations on state-of-the-art science and technology for the fabrication and characterization of Co–Cr films for PMR.

Before the review begins, it should be mentioned that three review articles have been written on the subject:

1. A brief and superficial review of thin-film media for magnetic recording was given by Eltoukhy [4], whose emphasis was "defining some of the general trends characteristic of most material systems and deposition technologies."
2. The review by Howard [5] on thin films for magnetic recording technology deals more seriously with the magnetization process and the physical principles underlying the PMR process. It covers magnetic thin films of almost all material systems for both perpendicular and longitudinal recording. Therefore, it lacks in-depth discussion of PMA films of the Co alloys.
3. Bonnebat [6] gives a review entitled "Information Storage Technologies – Some Recent Trend and Current Prospects Analyzed from the Media Manufacturer Standpoint." As the title suggests, the review is very general; it has no references listed.

2. Analysis

2.1. Magnetization and related phenomena in thin films with PMA

From the analysis of the demagnetization mechanism in short-wavelength magnetic recording, Iwasaki and Takemura [2] deduced (later confirmed by the Bitter technique) the so-called circular magnetization mode as contrasted to the conventional longitudinal mode. In the circular mode, remanent magnetization exhibits a closed-loop structure within the recording medium; it hinders high-density recording in longitudinal tape. These results led Iwasaki to propose a third, perpendicular, magnetization mode in thin films having their easy axes of magnetization oriented normal to the film surface. The motivation of his proposal was to achieve high-density magnetic recording.

An equally important element of Iwasaki's proposal was the selection of the Co–Cr alloy system for the preparation of thin films with PMA. The Co–Cr alloys were selected for several reasons. One is that the perpendicular anisotropy constant, $K_\perp$, exceeds the shape anisotropy energy or the demagnetization energy, that is,

$$K_\perp > 2\pi M_s^2 \quad (1A)$$

Recalling that the anisotropy field, as defined by [7], is

$$H_{K,\perp} = 2K_\perp/M_s \quad (2)$$

condition (1A) can now be converted to

$$H_{K,\perp} > 4\pi M_s \quad (1B)$$

To see how this condition is satisfied in the Co–Cr system, let us resolve $K_\perp$ into two components: the conventional magnetocrystalline anisotropy constant, K_u, and the shape anisotropy energy, $2\pi M_s^2$. Now we have

$$K_\perp = K_u + 2\pi M_s^2 \quad (3A)$$

or

$$K_u = K_\perp - 2\pi M_s^2 \quad (3B)$$

This first condition for the onset of PMA is then equivalent to having a positive value for K_u. For thin films of pure cobalt, K_u is normally negative. For bulk cobalt, however, the first and second magnetocrystalline anisotropy constants are positive: $K_1 = 0.43\ \mathrm{J\,cm^{-3}} \times 10^6\ \mathrm{J\,cm^{-3}}$ and $K_2 = 0.12\ \mathrm{J\,cm^{-3}} \times 10^6\ \mathrm{J\,cm^{-3}}$ at 20 °C [7]. Also claims were made for positive K_u values in thin films of pure Co [8, 9]. The negative value of K_u diminishes to zero as the addition of chromium approaches ~ 13 at % and becomes positive at higher concentrations. Referring to Equation 3B, besides the second-power dependence on M_s, alloying Co with Cr tends to decrease M_s more than $K_\perp$, thus leading to the onset of perpendicular anisotropy in Co–Cr films with more than 13 at % Cr. A detailed discussion on the composition dependence of K_u and M_s is in Section 3.2. Other advantages of Co–Cr films are discussed in Section 3.1.

Several workers analysed the mechanism of magnetization reversal in the PMA films. All analyses were based on two established processes: (i) rotation of the magnetization vector and (ii) domain-wall motion [7]. The stage at which a specific process dominates differed as the main variable in different analyses. Andra *et al.* [10] analysed the two processes separately. For the rotation process, the film is assumed as an infinite array of homogeneous ferromagnetic prisms. Physically, the prisms represent the columns, and it is assumed that the columns are separated by nonmagnetic gaps. The array is treated as two dimensional in the sense that the magnetization vector rotates only in the y–z plane parallel to the prism axis. This analysis yields oblique hysteresis loops with the shape of a parallelogram, and the main parameters such as reversal starting field, coercivity, and remanence can be calculated. The calculated results agree qualitatively with the observed loops. For domain-wall motion, Andra *et al.* assume that nucleation of 360° walls marks the start of magnetization reversal that causes jumps in the M–H plot reported by Kooy and Enz [11]. This type of Block wall, introduced by Kaczer [12], refers to two winding walls pushed together by an external field. They are stable at strong fields, thereby avoiding thresholds for wall nucleation. The analysis indicates that the nucleation and motion of the 360° walls contribute significantly to the mean magnetization during the approach to saturation.

Honda *et al.* [13] calculated the hysteresis loop of a perpendicular film as a function of the angle between the applied field and the axis normal to the film plane. The calculation was based on the assumption that both rotation of the magnetization vector and domain-wall motion occur concurrently and that lattice defects act as obstacles to wall motion. Good agreement was obtained between calculated and experimental results. Inhomogeneous rotation was shown as the major process of magnetization reversal in perpendicular films by Fedosyuk *et al.* [14]. This third analytic

work can quantitatively estimate the perpendicular coercivity for a range of film thickness and columnar grain size.

Applying the principles of micromagnetics, Soohoo [15] derived analytical expressions for wall energy density, wall width, and the magnetization distribution of domain walls of the simple Block type in vertical-recording media. To simplify the analysis, he assumes that the medium lattice is "homogeneous" (meaning featureless), rather than columnar in grain structure. The analysis shows that the magnetic transition zone in the media can be just the width of the wall, thus enabling the perpendicular recording to attain higher density than the longitudinal recording.

The electronic properties of close-packed hexagonal (h c p) $Co_{1-x}Cr_x$ alloys were studied theoretically by Nelson *et al.* [16], who applied the non-spin polarized mixed-basis self-consistent pseudopotential method. Total charge density, effective charge, and other characteristics of the band structures are calculated for $x = 0$, 0.25 and 0.5. The charge transfer from Cr to Co, which is about 0.04 electrons per Co–Cr bond, does not show large changes with stress. For $x < 0.25$, hence for all Co–Cr alloys involved in PMA films, the band structure of Co does not show significant changes with alloying.

2.2. Perpendicular magnetic recording (PMR)

Iwasaki [3] proposed the use of PMA films to attain high-density magnetic recording after he realized that the demagnetizing field, H_d, played an important role in the medium's performance. Not only does H_d decrease remanent magnetization, it causes rotation of the magnetization vector responsible for the circular-magnetization mode [2]. The latter mode gives rise to significant decreases of reproduction signals, thus disallowing high-density recording. In digital recording, there are noticeable differences in H_d between perpendicular and longitudinal modes. Assuming an isolated transition in perpendicular magnetization, the vertical component of H_d is given in the coordinate system shown in the inset of Fig. 1 as

$$H_{d,y} = 4M_r\left(\tan^{-1}\frac{x}{y-(\delta/2)} - \tan^{-1}\frac{x}{y+(\delta/2)}\right) \quad (4)$$

where M_r is remanent magnetization and δ is film thickness. Fig. 1 shows the variation of calculated values of $H_{d,y}/M_r$ with x/δ. Note that the perpendicular demagnetizing field, $H_{d,y}$, in the PMA film medium decreases to zero near the transition [17] or as the recorded wavelength is decreased [3]. These results led Iwasaki to conclude that, in principle, the perpendicular-magnetization mode can achieve the ideal step-change magnetization for the NRZI (non-return to zero, inverted) signal. In practice, however, it is expected that the length of the magnetization-transition region is controlled by grain size of the columns in the PMA films. The column size in sputtered Co–Cr films can be smaller than 0.1 μm in diameter. Accordingly we can expect a satisfactory recording resolution with densities up to about 1.2

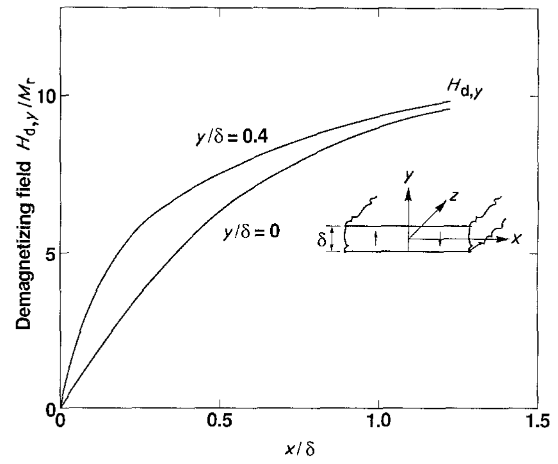

Figure 1 Demagnetizing field by an isolated transition of M_y.

$\times 10^5$ bytes cm^{-1} in the perpendicular-magnetization mode [18]. The complementary nature of perpendicular and longitudinal recording is illustrated in Fig. 2 [17].

In addition to the recording medium, another important element of PMR is the magnetic head, which must produce a field whose perpendicular component has an intensive and sharp distribution [17]. To this end, Iwasaki and Nakamura [3] initially used a special single-pole-type (SPT) head that consisted of a main pole of an electrodeposited Fe–Ni film in contact with the medium and a large auxiliary pole composed of 0.7 mm thick Mn–Zn ferrite on the other side of the medium. This asymmetric structure enables the SPT head to act as a perpendicular-type head because it produces a field that can be applied to the medium without tilt from the normal of the medium. In searching for the factors that limit the maximum density of PMR, they proved the conventional ring-type head having a narrow gap length of 0.67 μm to be effective [17].

Potter and Beardsley [19] conducted computer calculations using the self-consistent vector-field recording model [20]. Their results show that existing conventional SPT heads are suitable to couple with PMA media. At equal bit shift and 0.25 μm head-to-disk separation, perpendicular recording gives a factor of 2.5 increase in the linear density attained from media currently in use. Beardsley [21] later modified both the vector-hysteresis model and the two dimensional self-consistent recording model so that the analysis would be more applicable to PMA films operating in conjunction with a thin-film head. Beardsley's major modification lies in the astroid [7] by greatly increasing the anisotropy field of the crystallite to reflect the hard-axis behaviour. Remaining intact, however, is switching in the easy direction by nucleation of reverse domains at a field approximately equal to the coercivity. With the modification, the calculations predict an isolated pulse shape and amplitude in much agreement with experiment. Koehler [22] further refined the computer modelling of magnetic recording by introducing a fast, two dimensional vector-hysteresis model and by applying the finite-element method [23] to solve the electromagnetic problem

(a) Perpendicular Mode (b) Longitudinal Mode

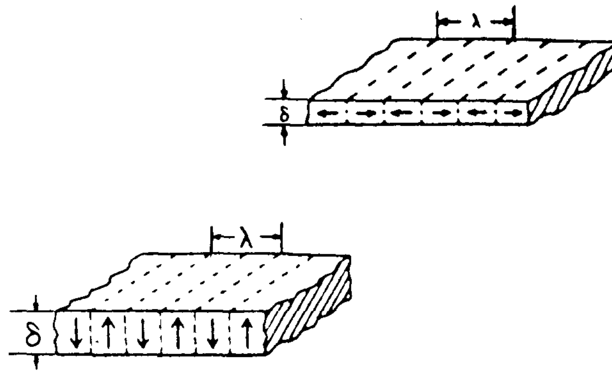

	λ → 0, H_d → 0	λ → 0, H_d → $4\pi M$
Medium-Anisotropy	Perpendicular	Longitudinal
—Film thickness	Thick	Thin
—Magnetic characterization	(1)High M_S (2)$K_\perp$(uniaxial)	(1)High H_C (2)$K_\parallel$(uniaxial)
Head	Single Pole-type (y-comp.)	Dipole (Ring)-type (x-comp.)
Signal	Digital (sat.)	Analog (non-sat.)
Recording method	Modulation (1M, PCM)	AC Bias method
Erase	DC Field	AC Field

Figure 2 Complementary features for perpendicular and longitudinal magnetic recording.

posed by the coupled system of current coil, recording head, and hysteretic recording medium.

The sharp transition of magnetization in perpendicular recording that Iwasaki proposed [18, 24] was investigated theoretically by Beardsley and Tsang [25]. Two models were adopted to represent different switching mechanisms: a simple continuum model for switching by domain-wall motion and a discrete model for switching by fixed needle-like domains. In the continuum model, the equilibrium magnetization distribution in the transition is assumed to correspond, in the absence of exchange energy, to the minimization of the sum of magnetostatic and uniaxial anisotropy energies. In the discrete model, the medium is assumed to consist of two dimensional columns packed along the downtrack direction. Both models predict a range of medium and head parameters for the onset of sharp transition. Also limiting the transition sharpness are such factors as the head field gradient in the discrete model and possibly the exchange interaction in both models. Nakamura *et al.* [26] later revealed analytically that the magnetic interaction between the main pole of an SPT head and the Co–Cr layer in the medium affects the bit-density response, the reproduced voltage, and the head-to-medium spacing loss. This analysis also reconfirmed the advantages of the double-layer structure in the medium for PMR [27, 28]. The presence of the soft magnetic underlayer reduces the relative thickness of the Co–Cr layer to that of the main pole of the SPT head, thereby leading to an enhancement of the high-density recording characteristics. The analyses of the head-medium coupling in perpendicular and longitudinal recording were reviewed in broad and somewhat empirical terms by Yeh [29]. It is concluded that control of the head-medium coupling for the optimization of the conditions of the medium and head is a key factor in designing a high-density recording system.

Two dimensional numerical analyses were performed on a PMR system of a double-layer medium containing a permalloy film and a ferrite composite head as sketched in Fig. 3 [30]. The formulation in these analyses is based on Poisson's Equation for the z-component of the magnetic-vector potential, A_z, in the system

$$\frac{\partial}{\partial x}\left(\mu^{-1}\frac{\partial A_z}{\partial x}\right) + \frac{\partial}{\partial y}\left(\mu^{-1}\frac{\partial A_z}{\partial y}\right) = -4\pi j_z - 4\pi(\mathrm{rot}M)_z \qquad (5)$$

where μ is permeability, rot M (rotational) magnetization of the medium with hysteresis, B magnetic induction, and j_z the z-component of the write current. Note in Equation 5, $\partial A_z/\partial y$ and $-\partial A_z/\partial x$ are B_x and B_y, respectively, where B is the magnetic induction. In the CGS system, for the main pole layer, underlayer, and ferrite substrate, B is related to the magnetic field from the definition of μ, ($\mu = B/H$), whereas for Co–Cr media:

$$B = H + 4\pi M \qquad (6)$$

Poisson's Equation is solved iteratively using a finite-element method with the boundary potential set at zero. The following conclusions are drawn:

1. The magnetomotive force needed to produce a sufficient perpendicular field in the medium is about 1/10 that involving the SPT head proposed by Iwasaki *et al.* [31].
2. The optimal spacing between the magnetic layer and the ferrite substrate in the head necessitates 5–20 times the distance between the main pole and the underlayer.
3. High-density PMR up to 4×10^4 bytes cm^{-1} is possible for the Co–Cr medium-thin-film head system.

Minuhin [32] compared theoretically the readback harmonic responses between perpendicular recording with a probe head over a medium having a permeable underlayer and longitudinal recording with a ring head. The readback performance was very different between the two and was dependent either on the distance, D, between probe tip and underlayer or on the medium thickness. The readback resolution of a probe head is inferior to that of a ring head unless the P/D ratio (P is probe thickness) is increased to approach 10. For small P/D ratios, the readback output of a probe is lower than that of a ring head.

The write process in PMR was investigated using a self-consistent computer simulation model [33]. The model is one dimensional because both the magnetization and the total magnetic field are considered only in the direction normal to the medium motion. The imaging from a highly permeable ring head is seen to affect the contact recording. After optimization, contact recording produces a positive slope in the magnetization spectrum, therefore enhanced frequency response. The analysis reached good agreement with the experimental data.

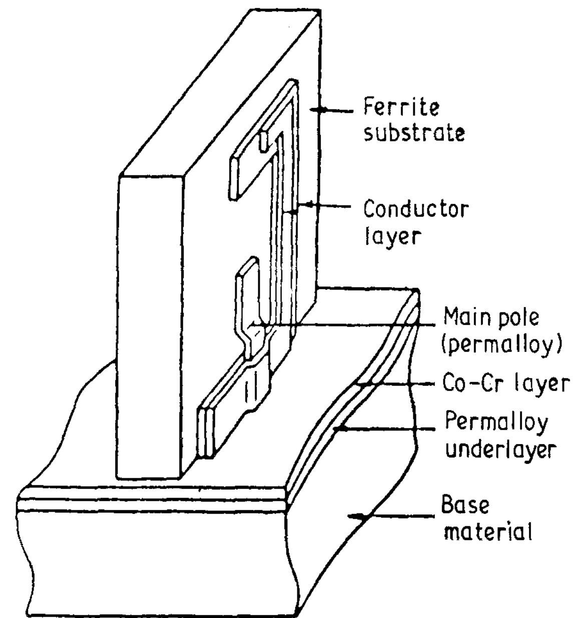

Figure 3 Schematic view of thin permalloy film/ferrite composite head and double-layer medium.

3. Selection of alloy systems for PMA films

Although Co–Cr alloys were chosen as the materials of the PMA films by Iwasaki [3], a survey of the literature reveals that many other alloys have been prepared with similar PMA. Up to now, however, Co–Cr alloys have dominated the PMR media and heads.

3.1. Criteria for alloy selection

Several criteria have been suggested for the selection of the PMA alloys:

1. The obvious and most crucial criterion is the *perpendicular magnetic anisotropy constant* $K_\perp$, which must be greater than either the shape anisotropy or the demagnetization energy, i.e., $K_\perp > 2\pi M_s^2$ (Equation 1A). As explained in Section 2, this condition is equivalent to demanding that the perpendicular anisotropy field be greater than the demagnetizing field, i.e., $H_{K,\perp} > 4\pi M_s$ (Equation 1B) and that the magnetocrystalline anisotropy constant, K_u, be positive. Fukuda *et al.* [34] reported the only exceptional case in which the Co–(8–26) at % V alloys exhibit PMA in RF-sputtered films without satisfying this critical condition.

2. The second criterion is the *crystal structure of the alloy*. If the alloy has an isotropic crystal structure, such as face-centred cubic (f c c) Ni alloys and body-centred cubic (b c c) Fe alloys, PMA will either not be developed or be developed without sufficient sharpness for PMR applications.

Hence, we establish the second condition that the lattice of the alloy must be anisotropic; the h c p lattice is ideal to meet this. In addition to a high degree of crystal structural anisotropy, h c p metals (e.g., Be [35]) and alloys display the natural tendency to preferential columnar growth with the c-axis oriented normal to the plane of vapour-deposited films. For Co and Co–rich alloys, this preferential growth also aligns the easy axis of magnetization normal to the film plane, thereby enhancing the PMA. Clearly the first and second conditions qualify cobalt as a unique base metal of PMA films. Other criteria for the PMA alloys are:

3. *Magnetic properties* – The saturation magnetization, M_s, and the perpendicular coercivity, $H_{c,\perp}$, must be sufficiently large to ensure high output voltage and high resolution in the recording [36]. However, M_s must be enough less than that of pure cobalt to satisfy Equation 3. Also the $H_{c,\perp}$ must not be too large to impair the recording efficiency.
4. *Wear and corrosion resistances* – Both must be improved with respect to those of pure cobalt.
5. *Sputtering yields or evaporation rates* – They should be comparable between the base metal and the solute.

Criteria (3)–(5) are not as important as the first two.

3.2. The cobalt–chromium system and modified alloys

The binary Co–Cr alloys constitute a basic system of materials that meet most of the five conditions above. Through torque measurements, Iwasaki and Ouchi [36] deduced K_u values that are listed in Table I with the M_s values for the Co–Cr alloys in the composition range that concerns us. At about 13 at % Cr, K_u vanishes from negative values. At higher Cr contents, K_u becomes positive and the inequality $K_\perp > 2\pi M_s^2$ holds. Hence, as far as the first condition is concerned, alloys with Cr content higher than 13 at % are suitable for making PMA films. Other magnetic properties and resistances to wear and corrosion of the Co–Cr alloys are discussed later.

Many attempts were made to modify this binary system. So far, nine elements in three categories have been tried; (i) Transitional elements: V, Ni, Nb, Mo, Rh, Ta, and W; (ii) Lanthanide: Pr; (iii) Nonmetallic element: C.

Smits and den Broeder [37] evaluated the ion-beam sputtered films of a series of $(Co_{90}Cr_{10})_{100-x}TM_x$ alloys, where TM = V, Nb, Mo, and Ta and x = (0–20) at %. They found that the V-doped films show coarse grains, leading to relatively low values of coercivity and poor [0001] texture, the Mo- and Ta-doped films deposited at 200 °C have fine grain size, leading to sharp [0001] texture and improved perpendicular anisotropy, and that the Nb addition produced amorphous structure and no PMA.

The positive effect of Ta on the c-axis texture was reaffirmed by Tamai *et al.* [38], who also observed improvements in the perpendicular anisotropy field and coercivity. The latter workers optimized the addition of Ta at 2.0–3.0 at % with 18 at % Cr. Allan and Fisher [39] evaluated the coercivity, static and dynamic friction coefficients, and recording performance of Co–12 at % Cr alloys doped with 2 at % Ta and of three other ternary alloys: Co–19 at % Cr–2 at % W, Co–30 at % Ni–7.5 at % Cr, and Co–22 at % Ni–10 at % W. All four alloys exhibit relatively high squareness and coercivity, with low friction and stiction (static friction) coefficients. These alloys are considered suitable for PMR. High coercivities were also reported for the Co–Ni–Cr alloys by Yamada *et al.* [40]. The latter study was extensive on the composition dependence of H_c and on the product of residual induction and film thickness. The addition of Ni to Co–Cr also improves the resistance to humidity. The authors claimed that the CoNiCr/Cr thin-film disc displays recording and reproducing properties equivalent to those of the CoNiP-plated disc. The addition of ~ 6 at % rhodium to Co–23 at % Cr sharpens the c-axis texture as evidenced by 20–40% decreases of the half-value width of the diffraction rocking curve, $\Delta\theta_{50}$, according to Kobayashi and Ishida [41]. A disc composed of a Co–Cr–Rh alloy deposited in single layer on an anodized aluminium substrate is capable of PMR at a density of 9200 flux reversal cm^{-1}.

TABLE I Saturation magnetization and anisotropy constants of the cobalt–chromium alloys [34]

Composition (at % Cr)	M_s (e.m.u. cm^{-3})	$2\pi M_s^2$	K_u ($J\ cm^{-3}$)	$K_\perp$ ($J\ cm^{-3}$)
0 (pure Co)	1410	124.9×10^5	-7.2×10^{-2}	117.7×10^{-2}
8.6	950	56.7×10^5	-1.6×10^{-2}	55.1×10^{-2}
10	850	45.4×10^5	—	—
13	700	30.8×10^5	0	30.8×10^{-2}
15.5	500	15.7×10^5	4.0×10^{-2}	19.7×10^{-2}
17	430	11.6×10^5	—	—
18.2	300	5.7×10^5	4.9×10^{-2}	10.6×10^{-2}
20	200	2.5×10^5	4.5×10^{-2}	7.0×10^{-2}

A recent study [42] of Co–Ni horizontal magnetic recording films had indicated that the addition of small amounts of Pr or Nd would affect the magnetic properties and improve the corrosion resistance. This prompted Suzuki and Yoshida [43] to evaluate the effect of Pr on the magnetic properties and microstructure of $Co_{0.80}Cr_{0.20}$. Indeed, M_s and $K_\perp$ are found to increase with the addition of Pr to a maximum at about 0.5%, followed by decreases at higher Pr concentrations. The microstructure also changed, resulting in less defined columnar growth.

Magnetic properties of the $(Co_{0.77}Cr_{0.23})_{100-x}C_x$ alloys, with x = 0–0.32 at %, were evaluated by Awano and Masuya [44]. The carbon doping tends to increase M_s because of an enhancement of Cr segregation and to either increase or decrease H_K and $H_{c,\perp}$, depending on the amount of carbon added, due largely to the change in K_u. In another study, Inoue *et al.* [45] found that the addition of 1% C to the Co–26% Cr–5% W films converts the complex alloy from nonmagnetic to ferromagnetic with a high degree of PMA and greatly improves the resistance to ring-type head abrasion. These remarkable changes in magnetic and mechanical properties are attributed to a preferential formation of carbide with Cr and to the refinement of grain structure.

3.3. Other alloys

Although binary alloys of the Co–Cr system are the dominant materials of PMA films, other alloys have been explored for their suitability to PMR applications. These other alloys can be classified into Co-base and Fe-base.

3.3.1. Other cobalt alloys without chromium

Three types of Co-base alloys without chromium have been developed. Their thin films show PMA and attractive magnetic properties suitable for PMR applications. Iwasaki *et al.* [46] were the first to report PMA in Co–V alloys. Later the Co–V alloys were studied by Fukuda *et al.* [34] and Thompson and Stevenson [47]. Both studies unveiled interesting phenomena. Fukuda *et al.* found that the Co–(8–26) at % V alloys develop PMA in RF-sputtered films even though the condition $H_{K,\perp} > 4\pi M_s$ (Equation 1B) is not satisfied. In the other study, RF-sputtered films of Co–17 at % V are either amorphous or crystalline with the [0001] texture and show widely varying perpendicular coercivity from $< 7.9 \times 10^3\ Am^{-1}$ to $> 1.08 \times 10^5\ Am^{-1}$, depending on whether or not a

bias voltage, i.e., $V_b = 0$ or -100 V, is applied to the glass substrate.

Carcia [48] evaluated the second type of Co alloys, which contain Pd or Pt in the form of layered films with modulated composition. RF-sputtered films consisting of separate layers of Co and Pt or Pd display PMA when the Co layer is very thin (< 0.8 nm in Pd/Co, < 1.4 nm in Pt/Co). The formation of PMA in the layered films of Co/Pd and Co/Pt is ascribed to an interfacial anisotropy and the mixing at the interface of Co and Pt atoms, respectively. Carcia's study has more scientific interest than technological value, however.

PMA was detected in the Co–CoO films prepared by reactive RF-sputtering in argon-oxygen mixture by Ohkoshi *et al.* [49]. The film is copmposed of hcp ferromagnetic Co particles in columnar form and fcc antiferromagnetic CoO particles. The observation of PMA in these Co–CoO films is interesting for two reasons. First, the case seems to present an exception to the first condition for the onset of PMA discussed in Section 3.1. Note that Co is the only ferromagnetic material responsible for the PMA in the films. Second, as might be expected, oxygen contamination of the Co–Cr films leads to the deterioration of PMA and an overall degradation of PMR characteristics [50]. Above a critical partial pressure (99.98 to 133.3 mPa, depending on the deposition rate) of oxygen, the film is predominantly of the Co_3O_4 single phase, which is not ferromagnetic.

3.3.2. *Iron-base alloys*

The motive for shifting the PMA alloys from Co-base to Fe-base was to reduce the demagnetizing field by means of lower magnetization. Desserre and Jeanniot [51] alloyed Fe with Tb and Gd, in the composition range $Fe_{1-x-y}Tb_xGd_y$, where $x \simeq y$ and $x + y =$ 15–30 at %. The sputtered films are amorphous and show PMA with higher squareness than that attained in the Co–Cr films. More recently, Berstein and Rio [52] prepared amorphous Fe–Tb and Fe–Gd films by the *e*-beam co-evaporation process and characterized the PMR performance of the Fe–Tb(Gd)-film media.

Another type of Fe-base thin-film alloys that are capable of producing PMA contain oxygen with or without a third element in the formula Fe_xO_{1-x} and $Fe_xE_yO_{1-x-y}$, where E is either a nonmagnetic element such as Si [53] and Sn [54] or a magnetic element such as Co [53]. Thin films of Fe–Co–O and Fe–Si–O show increasing M_s with decreasing oxygen content below 50 at %, i.e., $1 - x - y < 0.5$. The films also show strong PMA, thus overwhelming the shape anisotropy in certain composition ranges. All these alloys with proper oxygen and Co or Si concentrations are suitable for PMR applications.

Hexagonal Ba–ferrite films of the magnetoplumbite type [7] were prepared in an RF-diode sputtering system by Morisako *et al.* [55]. The ferrite films feature good *c*-axis texture and smooth surfaces. Rigid discs made of such films were evaluated with a ring-type head. PMR capabilities with recording densities $D_{50} = 4330$ and 7480 kilo flux reversal per metre (kFRPM) were demonstrated for $\Delta\theta_{50} = 4.8°$ and 2.8°, respectively.

4. Fabrication of PMA films

4.1. Physical vapour deposition (PVD) by sputtering

Iwasaki and Ouchi [36] applied the sputtering process in their initial experiments for the fabrication of Co–Cr films featuring PMA. Not only were the experiments successful, they demonstrated that sputtering could be an effective and convenient technique. Their success, coupled with the outstanding features of the process, explains why sputtering is so popular in this development. Comparing with other film-fabrication processes, such as evaporation (Section 4.2) and electroplating (Section 4.3), sputtering offers the great advantage that it has many operational parameters that can be varied or adjusted over a wide range [56]. Hence, by optimizing these parameters, we can prepare high-quality PMA films to meet the stringent requirements outlined in Section 3.1. The alterable or adjustable parameters include:

1. Sputtering mode (RF or d.c.).
2. Design and geometric arrangement of the target(s).
3. Method of generating ions (glow-discharge or ion-beam).
4. Pressure of argon.
5. Voltage and power for sputtering.
6. Material, temperature, and bias voltage of the substrate.
7. Techniques for special effects.

Indeed, all these parameters have been evaluated and optimized for sputtering the Co–Cr alloys. Another advantage of sputtering is the ease with which the surface of the substrate can be cleaned prior to deposition *in situ* by sputter or ion-beam etching. Hence, it enables more efficient cleaning than do processes performed outside the sputtering chamber. Smits *et al.* [57] and Thompson and Mee [58] showed that thorough cleanliness and good finish of the substrate surface are essential in the production of the sharp [0001] texture required for strong PMA.

The sputtering process has thus far been performed in four different modes of implementation: RF diode; d.c. magnetron; ion beam; special techniques for high-rate deposition.

4.1.1. *RF-diode sputtering*

Although RF- and d.c.-sputtering have both been used for fabricating PMA films, the selection of the two modes is made here according to the specific technique used for sputtering. For example, for the conventional diode sputtering, RF is the choice because d.c.-diode sputtering is too slow in deposition. For magnetron sputtering, however, d.c. is preferred so as to simplify the operation.

Iwasaki and Ouchi [36] prepared the first PMA films of Co–Cr alloys by sputtering in the RF-planar-diode mode. Subsequently, Coughlin *et al.* [59],

Wielinga and Lodder [60], Lodder *et al.* [61], Thompson and Mee [58], and Maeda [62] all applied sputtering in the same RF-diode mode to fabricating the PMA films of Co–Cr. The planar target serves as one electrode, the substrate is in contact with the other electrode, and plasma is generated between the two. This sputtering geometry is the simplest and probably the most widely used configuration [63]. In addition to higher deposition rates, RF was chosen here for the advantage that RF discharge in planar-diode apparatus can be operated at considerably lower pressures than can d.c. discharge [63]. Indeed, Wielinga and Lodder [60] found that "for increasing Ar pressure, the *c*-axis of the h c p structure gradually declines from normal to in-plane orientation." In other words, development of the preferred orientation for PMA necessitates the use of low argon pressure. The argon pressures used in the various studies except [62] fall in the 0.1–1.33 Pa range, in contrast to the 6.65–13.3 Pa argon pressure required to sustain glow discharge generally in d.c.-planar-diode sputtering [63].

Targets used in the RF-diode mode are discs constructed of either Co–Cr alloys of predetermined compositions or pure cobalt discs with the front surface partially covered with Cr pellets in proportion to the desired nominal composition.

The operational conditions for RF-diode sputtering varied in a narrow range in various studies but [62]:

Argon pressure	0.4–1.33 Pa
Background pressure	Below 2.66–7.98 $\times 10^{-5}$ Pa
Target voltage	1500–1600 volts
Sputtering power	100–360 watts
Substrate temperature	150–170 °C

Under these conditions and for unspecified target-to-substrate distances (except in [60], which was cited at 55 mm), the deposition rate is around 0.2 nm s^{-1} (or equivalently 0.72 μm h^{-1}). This is a very low rate. Maeda [62] attained higher deposition rates, 0.3–0.5 nm s^{-1}, using much higher argon pressures at 3.2–9.3 Pa.

Other common features of the various RF-diode sputtering practices reported include:

1. Bake the vacuum chamber to attain low background pressure.
2. Clean the substrates (except polyimide substrates) by sputter-etching.
3. Presputter to avoid contamination of the initial deposition in the film.
4. Preheat all but polyimide substrates up to 170 °C to ensure good adhesion.

Thompson and Mee [58] studied the effect of RF voltage changing from 1.0 kV to 1.5 and 2.0 kV on the microstructure of $Co_{0.8}Cr_{0.2}$ films. Unfortunately, their experiments were statistically designed so that four other parameters (Ar pressure, film thickness, substrate bias, and time for sputter-etching) were also varied. Therefore the voltage effect was not sorted out.

4.1.2. D.c.-magnetron sputtering

Although RF-planar-diode sputtering can fabricate PMA Co–Cr films of good quality for PMR, its deposition rate is considered too low to meet mass-production demands. Consequently, Kadokura *et al.* [64] were the first to apply d.c.-magnetron sputtering in the "opposing-targets" configuration in 1981. The deposition rate was increased to 5.0–6.67 nm s^{-1} (or 18–24 μm h^{-1}), which is 25–33 times the 0.2 nm s^{-1} rate generally observed in RF-diode sputtering. The films of Co–18.5 at % Cr thus fabricated displayed sharp PMA with $\Delta\theta_{50} = 3°$ and other good magnetic properties: $H_{c,\perp} = 87\,538$ A m^{-1}, $H_K = 453.6$ k A m^{-1}. Other workers, notably Roll *et al.* [65], Iwasaki *et al.* [66], Ravipati *et al.* [67], and Kume *et al.* [68] applied d.c.-magnetron sputtering in either the (conventional) single-target or the opposing-targets configuration.

In addition to increasing the deposition rate, magnetron sputtering offers the advantages of larger deposition area, lower discharge voltage, and less substrate heating. The increase in deposition area is particularly attractive for industrial applications. In a pioneer study, for example, Mayr *et al.* [69] were able to deposit Co–19 at % Cr onto polyimide web up to 1.2 m wide in a two-sided d.c.-magnetron-sputtering roll coater equipped with eight sputter cathodes. It is doubtful that such large substrate width can be handled by other sputtering means with equal efficiency.

The deposition rate in the d.c.-magnetron sputtering of the Co–Cr alloys ranged from 1.1 nm s^{-1} (~ 4 μm h^{-1}) to as high as 31.7 nm s^{-1} (or 114 μm h^{-1}) under the following conditions:

Argon pressure	0.1–1.33 Pa
Background pressure	6.65 $\times 10^{-4}$ Pa
Sputtering power	15–50 W cm^{-2} or 500 W
Substrate temperature	Room temperature or 125–170 °C

Note that the argon pressures used in RF-diode and d.c.-magnetron sputtering of the Co–Cr alloys are in the range from 0.1–0.4 to 1.33 Pa. In a special case, Niimura *et al.* [70] used only 0.01 Pa pressure in d.c.-magnetron sputtering using opposing-targets. The low argon pressure was claimed to minimize the role played by the incidence angle, thus allowing the *c*-axis to be more preferentially oriented normal to the film plane even though the incidence angle was $< 45°$.

In both modes (RF-diode and d.c.magnetron) of sputtering, the quality of the background pressure (P_0) is extremely important for the attainment of sharp [0 0 0 1] texture and strong PMA. The reason is threefold; first, the lower the background pressure, the less contamination the film suffers; second, when the sputtering chamber is insufficiently oxygen-free, there is a better chance for surface-oxidation of the substrate, thus jeopardizing the chance of developing the texture for PMA; third, and perhaps the most important, Coughlin *et al.* [71] and Mayr *et al.* [69] reported that the presence of nitrogen in trace amounts, also oxygen to a lesser degree (but not hydrogen [69]), tends to destroy the columnar microstructure essential for formation of the [0 0 0 1] texture and promotes the formation of f c c phase leading to a longitudinal component in the magnetic anisotropy.

The P_0 value should be kept $< 6.65 \times 10^{-4}$ Pa, preferably $< 6.65 \times 10^{-5}$ Pa. Actually, such back-

ground pressure is not difficult to attain modern vacuum systems. As a precaution, Iwasaki and Ouchi [36] and Mayr *et al.* [69] specifically recommended that the sputtering chambers and the substrate holders should be baked at 300 °C.

In general, the operation of magnetron sputtering becomes difficult, if not impossible, for ferromagnetic targets because the targets tend to short-circuit the magnetic flux lines, thereby preventing the magnetic field from emerging on the target's front surface [72]. For the magnet to function properly, it must be sufficiently strong to saturate the target magnetically, and the magnetic flux lines must penetrate the target to produce a field of the desired shape on its front face [35]. If these conditions are not met, the magnetron glow discharge is not sustained, and the assembly is reduced to a pure diode with all the well-known disadvantages of d.c.-diode sputtering: low deposition rate, high discharge voltage, high substrate heating caused by electron bombardment [72]. These requirements require that the permanent magnet be strong relative to the M_s of the target material and that the target be thin enough to facilitate penetration by the magnetic flux lines. Since M_s of the Co–(18–25) at % Cr alloys are low, permanent magnets made of Fe–Nd–B or Co–Sm would have no problem saturating the Co–Cr targets. Even with a stronger magnet, however, optimal thickness of the Co–Cr disc targets is limited to 5–6 mm [65], much thinner than a normal nonmagnetic target. The life of such thin Co–Cr targets is short. Moreover, typical utilization of targets in standard magnetron design consumers only 20–30% of the mass, implying extremely short life of the Co–Cr targets and high cost for the fabrication of PMA films. Kukla *et al.* [72] designed a special magnetron assembly that allows target thickness to be increased 2–3 times (up to 14 mm) and the target life prolonged to 53% of the Co–19 at % Cr targets. The design is called interpole target for ferromagnetic (IPT/F) materials. As shown in Fig. 4, the IPT/F cathode consists of three elements: target, outer pole piece, and inner pole piece, all constructed of the same Co–Cr alloy. The total magnetic flux from the permanent magnet splits into three parts. Part 1 forms the short-circuit through the target and produces no magnetron effect. Part 2 runs through the nonmagnetic pole-piece mountings and the inner pole piece to the target; it produces a magnetron effect only in the vicinity of the pole pieces. Part 3 forms an arch of flux lines from the inner pole piece over the whole target area to the outer pole piece, which is of opposite magnetic polarity. This part produces a magnetron confinement of the plasma over the whole target surface. In such construction, sputtering of the pole pieces would not contaminate the deposit. The maximum input power for operating this magnetron is limited only by the ability to cool target, pole pieces, and permanent magnet – especially important for the Fe–Nd–B magnet on account of its relatively low Curie temperature. For the Co–Cr alloys, the maximum power density for continuous operation is $50\ \mathrm{W\,cm^{-2}}$. The IPT/F cathode can sputter thick ferromagnetic targets (besides Co–19 at % Cr, Ni–19% Fe of much higher M_s was also tested successfully) with high rates (10.0–$18.5\ \mathrm{nm\,s^{-1}}$) and extremely high target utilization (50–60%). The deposits were homogeneous in composition, $< 5\%$ fluctuation over a width of 1.12 m.

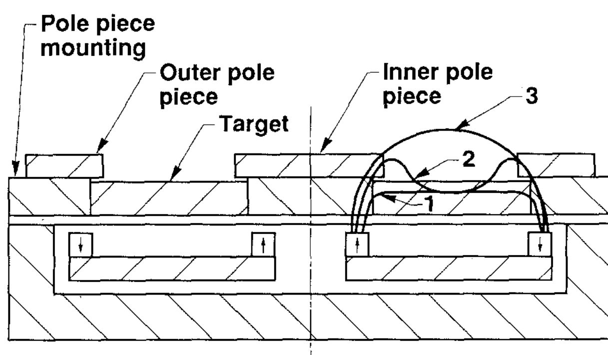

Figure 4 Magnetic-flux splitting of IPT/F cathode.

Three special-effect techniques have been applied to improving the properties of PMA films. One technique involves the application of a moderate (≤ 100 V) negative d.c. voltage to the substrate during sputtering. The advantages of bias sputtering have been discussed by Thornton [63] and Chen and Alford [35]. For the Co–Cr films, Ohkoshi and Kusula [73] observed pronounced effects of bias voltage on the [0 0 0 1] texture, grain size, perpendicular coercivity, and Q factor, where $Q = K_u/2\pi M_s$. Niimura *et al.* [70] detected the suppression of columnar growth by the bias voltage. This is in accord with the results for Be reported by Chen and Alford [35] but contrasts with the findings of Suzuki *et al.* [74], who applied a bias voltage varying from -500 to $+1400$ V to the polyimide substrate. In the latter study, transmission electron microscopy (TEM) examination of the $Co_{80}Cr_{20}$ films revealed that films prepared under high positive bias voltage showed columnar structure but that those under no bias showed only coarse grains without clear columnar structure.

Another special-effect technique is reactive sputtering involving oxygen or nitrogen. Maeda [62] and Thompson and Stevenson [75] reported the same phenomenon; oxygen added to Co–Cr reacts preferentially with Cr, leading to a deletion of Cr from the solid solution and an increase in M_s. Incorporating nitrogen [71] and, to a lesser degree, oxygen in Co–Cr tends to destroy columnar grain structure and to induce an in-plane f c c phase at the expense of the desired h c p phase, thereby weakening the PMA and increasing the perpendicular coercivity [75]. Nakatsuka *et al.* [76] and Honda and Uchiyama [77] reported another, somewhat positive, effect of oxygen; reactive sputtering caused formation of a protective surface layer of the Co–Cr film. The various effects of oxygen must be carefully sorted out before reactive sputtering is attempted. A third technique for special effect is the application of a magnetic field parallel to the sputtering electric field. Maeda [62] showed that a $119.6\ \mathrm{Am^{-1}}$ magnetic field could reduce $\Delta\theta_{50}$ from 8° to 3.5° and increase perpendicular hysteresis loop squareness significantly.

4.1.3. Ion-beam sputtering

In glow-discharge sputtering, the target and substrates are exposed to the plasma. Hence, target current density and voltage are closely related to the sputtering-gas pressure, signifying that they cannot be independently controlled [63]. To circumvent this, we can use a separate ion source, from which a beam of ions is extracted to impinge upon the target at a much lower gas pressure. Typical geometric arrangement of the ion gun, target, and substrate is shown in Fig. 5 [74]. Ion-beam sputtering permits independent control of the energy and current density of the bombarding ions [78]. For fabricating PMA films, ion-beam sputtering offers several advantages over the conventional sputtering process: better control of ion energy and current, lower gas pressure, independent beam-incidence angle, and more flexibility in the selection of the bombarding particles. Several authors [79, 80] have thus reached the verdict that the ion-beam technique provides more favourable choices of experimental parameters than are possible in conventional sputtering. A case in point is the work of Suzuki *et al.* [74], who detected less contamination by oxygen at lower argon pressure and less substrate heating caused by ion bombardment than in conventional sputtering. In this and another case [79], the versatility and manoeuvrability of ion-beam sputtering were vividly demonstrated by the improvements in the magnetic properties of the PMA films from better control of the major parameters. The technique may not be applicable to mass production because of the limited number and size of ion beams that can be used together.

The conditions for ion-beam sputtering are listed below. Note the differences from those practiced in conventional RF-diode and d.c.-magnetron sputtering:

Accelerator voltage	600–1800 V
Beam current	70–180 mA
Argon pressure	$2.7 \times 10^{-3} - 2.7 \times 10^{-2}$ Pa

Four studies using ion-beam sputtering detected pronounced effects of substrates on magnetic properties and microstructures of the Co–Cr films [57, 74, 79, 80]. Both material and temperature of substrates contribute to the effects. Gill and Rosenblum [79] deposited Co–18 at % Cr on four different substrates: chromium, titanium, glass, and amorphous Ta–W–Ni. They found that *c*-axis dispersion for film thickness ~ 200 nm was largest for films deposited on glass and chromium, and smallest on amorphous Ta–W–Ni and titanium. Co–Cr films deposited on the latter two substrates exhibited a transformation from multi-oriented grains to a single [0001] orientation at an earlier stage of the growth process than did films deposited on glass. The effect of substrate temperature, T_s was broadly evaluated by Smits *et al.* [57], who varied T_s from 50 °C to 400 °C. Increasing T_s would (i) improve the sharpness of the [0001] texture and the ratio of perpendicular-to-parallel squareness of the hysteresis loop, (ii) decrease the grain size, and (iii) increase the perpendicular coercivity from $300\,\mathrm{A\,m^{-1}}$ at $T_s = 50$ °C to $1.6 \times 10^5\,\mathrm{A\,m^{-1}}$ at $T_s = 400$ °C. The first and third effects of T_s were similarly arrived at by Maloney and Lustig [80], who also recorded a striking improvement of the ratio of perpendicular-to-parallel squareness of the hysteresis loop by increasing T_s. Smits *et al.* [57] emphasized that perpendicular anisotropy appeared only when T_s exceeded 150 °C. Precisely the same T_s had been cited by Wielinga and Lodder [60] in a study involving RF-diode sputtering: "An exclusive perpendicular orientation would be formed only when $T_s \gtrsim 150$ °C, and at lower T_s, an additional h c p phase appeared with in-plane *c*-axis orientation." It is more than coincidence that both studies point to 150 °C as the critical substrate temperature in developing the [0001] texture in the Co–Cr films. The additional h c p phase cited by Wielinga and Lodder [60] has never been mentioned by other workers. This controversy will be further discussed in Section 5.1.1, Phase identification, and in Section 5.1.3, Grain orientation and columnar growth. (increase) of the Curie temperature, θ_c, of films of fixed overall composition on (rising) T_s." They related this phenomenon to the promotion of segregation of Cr by increasing T_s. Deleting Cr from the Co–Cr phase to form islands of a Cr–rich phase will increase θ_c of the Co–Cr alloys to approach that of pure Co. This is a natural consequence of making the film more inhomogeneous at higher T_s. This segregation tendency of Cr in the Co–Cr films with rising T_s was reconfirmed by Maeda [62] and Fisher *et al.* [81] but not by Suzuki *et al.* [74], who speculated that "nearly uniform composition distribution occurs by Cr diffusion at high (substrate) temperature."

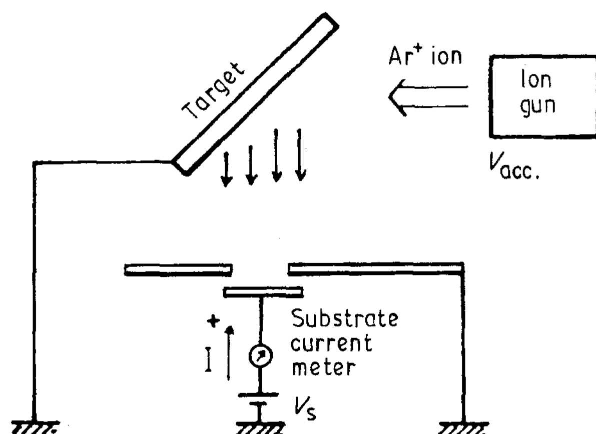

Figure 5 Geometric arrangement of ion gun, target and substrate.

4.1.4. Special sputtering techniques for high-rate deposition

As far as can be determined in the literature, Kadokura *et al.* [64] were the first to apply a special method for high-rate sputtering. Their method still basically relied on d.c.-magnetron sputtering with the innovation that two targets are used. As shown in Fig. 6, the two planar targets, identical in composition and dimensions, are facing each other, thus the terms opposing-targets [64] or facing-targets [57, 70] sputtering (FTS). Behind each target is a circular permanent magnet. The two magnets have their polarities arranged in the S–N–S–N sequence so that the flux lines

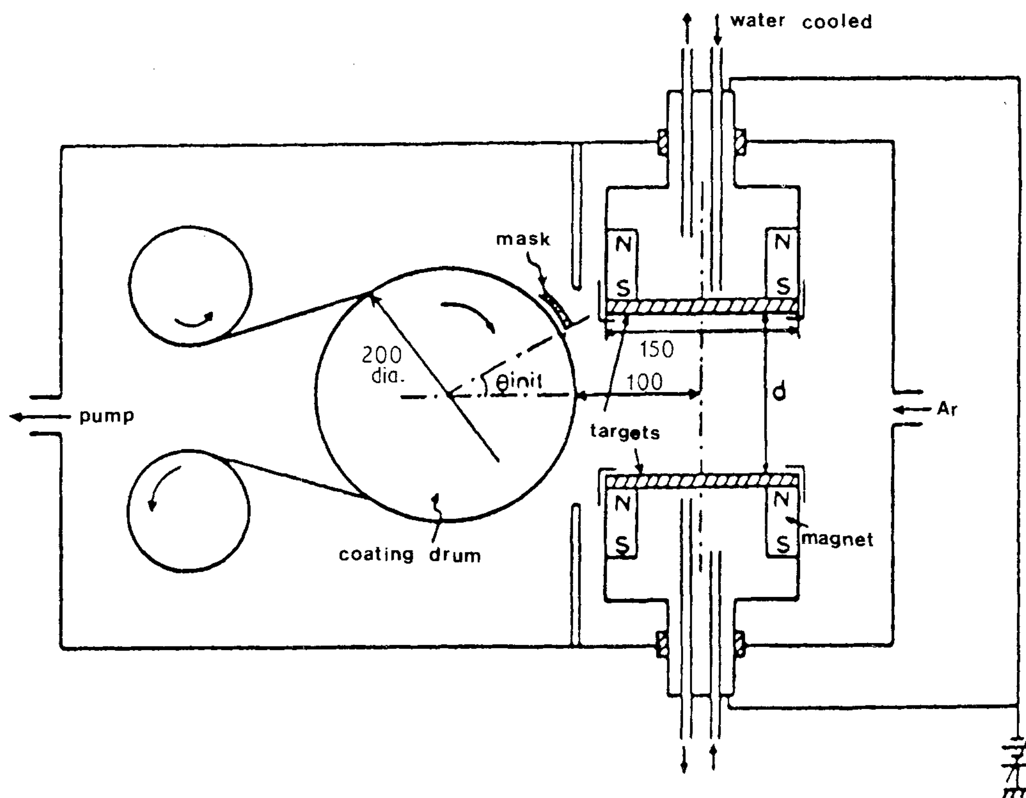

Figure 6 Schematic diagram of the targets-facing type of sputtering apparatus.

flow continuously in the direction normal to the target planes. This layout is capable of confining, in the space between the targets, the secondary electrons emitted as a result of ion bombardment from the front surface of the magnetron cathode. In this way, the ionization process is greatly enhanced and high-rate sputtering is realized. Note in Fig. 6 that the substrate is placed just outside the magnetic flux zone, and the closest surface section of the substrate to be coated is 100 mm from the central line of the two facing targets. This layout has another advantage in that the substrate film is not bombarded by electrons. Therefore, the problem of substrate heating leading to an undesirable temperature increase or fluctuation is avoided.

In the original facing-targets sputtering, with argon pressure at 0.5 Pa Kadokura and Naoe [82] attained moderate-to-high deposition rates that varied from $0.67\ \mathrm{nm\,s^{-1}}$ (or $2.4\ \mu\mathrm{m\,h^{-1}}$) to $6.67\ \mathrm{nm\,s^{-1}}$ (or $24\ \mu\mathrm{m\,h^{-1}}$) at 200 W and 1350 W, respectively. The Co–Cr films thus prepared exhibited good magnetic properties ($\Delta\theta_{50} = 3°$, $H_{c,\perp} = 7.6 \times 10^4\ \mathrm{Am^{-1}}$, $H_K = 3.8 \times 10^2\ \mathrm{kAm^{-1}}$) under zero bias voltage. Apparently, films prepared by this high-rate d.c.-magnetron sputtering process did not suffer magnetically. Moreover, the latter workers also claimed that "the FTS produced a different type of Co–Cr films in morphology." Unlike RF-diode sputtering and evaporation deposition, the FTS-produced films show no columnar growth, thus improving their suitability for PMR application. Their claim may be questioned for the fact that the bias voltage could also suppress columnar growth, as Chen and Alford [35] have described. This controversy will be discussed later.

The FTS method was further innovated by installing a winding system so that long (100 m) polyimide or PET tape substrates could be coated continuously [68]. The winding system consists of two small drums to load and unload the roll of the polymer tape and a larger drum, heated to 170 °C, for coating (Fig. 6). Largely by increasing the sputtering power density up to $47\ \mathrm{W\,cm^{-2}}$ and, to a lesser degree, by decreasing the target-to-target distance to 10.0 cm and the distance from the east line on the coating drum to the edge of the targets to 2.5 cm, the deposition rate was increased to a rate of $31.7\ \mathrm{nm\,s^{-1}}$ (or $114\ \mu\mathrm{m\,h^{-1}}$). The apparatus shown in Fig. 6 is similar to the "roll coater system" [77, 83], except that different types of targets were used. While Kadokura *et al.* [64] preferred their twin targets in the opposing configuration, Iwasaki *et al.* [66] and Honda and Uchiyama [77] used a conventional planar target for the Co–21% Cr alloy and a gap-type target [84] for Cu–Mo or Mo permalloy. The permalloy is deposited as the underlayer in a double-layer medium.

Workers at Laybold-Heraeus GmbH in West Germany approached the deposition-rate problem differently by designing the IPT/F discussed in Section 4.1.2. Operating the IPT/F at a maximum power density of $50\ \mathrm{W\,cm^{-2}}$, Kukla *et al.* [72] attained a deposition rate of $18.5\ \mathrm{nm\,s^{-1}}$ ($66.6\ \mu\mathrm{m\,h^{-1}}$) for coating polyimide web that is 1 m wide and 75 µm thick. The production machine, called a two-sided sputter roll coater, was described by Mayr *et al.* [69]. The huge coater consists of a rectangular 3.1 m × 2.3 m × 2.1 m stainless steel chamber divided into three sections: one winding section and two coating sections. A drive system unwinds the web from the original roll to start the procedure. The web first goes through a glow-discharge cleaning station, then is transported around the first 1 m diameter, coating

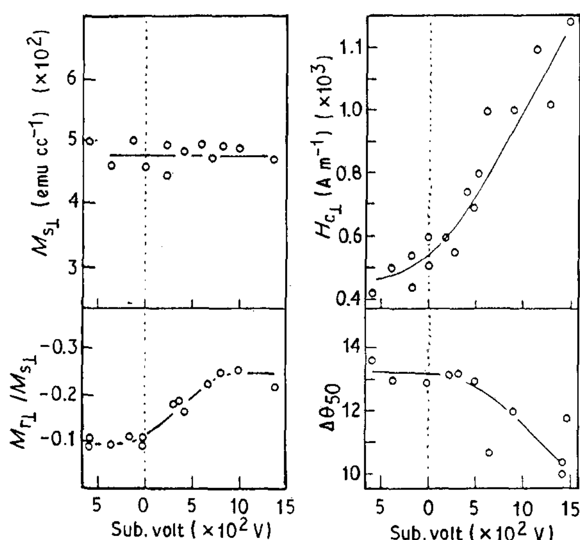

Figure 7 Substrate bias voltage dependence of $M_{s,\perp}$, $M_{r,\perp}/M_{s,\perp}$, and $\Delta\theta_{50}$ [74].

drum, and passes the plasma zones of four magnetrons. After finishing the front-side coating, the web is turned around through a guiding roll, pretreated again by glow discharge, coated on the backside in the second coating station that is also equipped with four magnetrons, and rewound. The productivity of the machine depends on layer thickness. One example was cited for 0.5 μm coating on both sides of a 6100 m web length at the production speed of $2\ \mathrm{m\,min^{-1}}$. The coated web displayed excellent transverse uniformity of H_K and $H_{c,\perp}$.

Before we leave the subject of sputtering, the effects of bias voltage and incidence angle should be discussed. Several workers have examined changes in magnetic properties or microstructures of the PMA films caused by the application of a bias voltage to the substrate. Ohkoshi and Kusuda [73] conducted probably the most comprehensive study of the effect of substrate bias voltage (0 to − 350 V) in the RF-diode sputtering mode. They found the following significant changes in grain structure and magnetic properties of the Co–Cr films:

1. The deposition rate gradually decreases at the rate of $0.03\ \mathrm{nm\,min^{-1}\,V^{-1}}$ after the negative bias voltage exceeds 100 V. This decrease is due primarily to resputtering of the deposited atoms in the film.

2. The size of grains in the Co–Cr films first increases from 20 nm in diameter at zero bias to 100 nm at − 40 V bias, then decreases to 10 nm at − 100 V bias. The grain-coarsening effect is ascribed to the suppression of oxygen contamination because of the ion-bombardment effect leading to a preferential resputtering of weakly absorbed oxygen and to an electrostatic effect in which negatively ionized oxygen produced in the plasma was repelled by the anode potential [85, 86]. For Be, however, as Chen and Alford [35] described, resputtering of the deposited film leads to grain refinement. In the present case of the Co–Cr alloys, preferential resputtering of oxygen seems to overshadow the other effect of bias on grains at lower bias voltage. Not until the bias voltage is increased to − 100 V would the grain-refining effect become apparent.

3. The intensity of the (0 0 0 2) peak in X-ray diffraction patterns and $\Delta\theta_{50}$ in the rocking curve become sharper and of lower value, respectively, with increasing bias voltage and reach a maximum and a minimum, respectively, at − 75 V. Above − 125 V, the (0 0 0 2) diffraction is not observed and the weak (1 0 0 0) peak is slightly intensified. These changes are attributed to an increase in surface mobility of adatoms, which promotes the most densely-packed (0 0 0 2) plane lying parallel to the substrate surface.

4. At − 75 V bias, the perpendicular coercivity decreases markedly, and a clear shoulder is seen in the hysteresis loop, suggesting reverse domain nucleation. Above − 125 V bias, the easy axis of magnetization changes from the original normal to the in-plane direction.

5. M_s decreases gradually with increasing bias, and approaches the value for the bulk alloy with biases > − 125 V. The initial decrease in M_s is related to a microscopic homogenization of composition induced by the bias voltage. Evidence of compositional inhomogeneity is seen in the higher M_s value for films sputter-deposited at zero bias and also in the higher Curie temperature for the zero-bias sputtered films.

6. The perpendicular magnetic anisotropy constants, $K_\perp$, decreases with increasing bias voltage and becomes zero in the high-bias region. However, the quality factor, $Q = K_\perp/2\pi M_s^2$, increases at − 75 V bias because of the rapid decrease in the demagnetizing energy, $2\pi M_s^2$, with increasing bias voltage.

To account for these property and microstructure changes, Ohkoshi and Kusuda [73] invoked a number of mechanisms and phenomena, including:

(i) Resputtering of the Co and Cr atoms in the growing film.

(ii) Preferential resputtering of oxygen atoms trapped in the film.

(iii) Enhanced argon-ion bombardment at moderate (− 40 to − 75 V) bias voltages, which induce more substrate heating and increase mobility of adatoms on the film surface.

(iv) Elimination of compositional inhomogeneity due to enhanced surface diffusion of the adatoms.

(v) Changes in physical properties in crystalline metallic films under the bias voltage.

Such diverse interpretations are tailored merely to explain a wide variety of property changes. Moreover, the observations were complicated by a significant increase of the substrate temperature from 150 °C at zero bias to 300 °C at − 150 V bias. For $H_{c,\perp}$ and M_s, the effect of T_s is known to be opposite to that of the bias voltage [85, 86]. Without isolation of variables, it would be difficult to gain an integral understanding of the basic mechanisms only from studies like the one conducted by Ohkoshi and Kusuda. In another study, Thompson and Mee [58] purposely varied the substrate bias voltage at 0, − 50, and − 100 V together with four other variables in a statistical-design study.

In the latter study, it is even more difficult, if not entirely impossible, to single out the effect of different variables. In fact, the latter workers failed to discuss the effect of the substrate bias. A more clear-cut situation existed in the study of Suzuki *et al.* [74] who prepared Co–20 at % Cr films by ion-beam sputtering with substrate bias voltage varying from -600 to $+1500$ V. The dependence of $M_{s,\perp}$, $M_{r,\perp}/M_{s,\perp}$, $H_{c,\perp}$, and $\Delta\theta_{50}$ on the substrate bias voltage is shown in Fig. 7. Negative bias tends to decrease $H_{c,\perp}$ as reported by Ohkoshi and Kusuda [73], but it exerts no influence on the other three properties. With increasing positive bias voltage, $M_{r,\perp}/M_s$ increases to a peak value that is unchanged beyond 1000 V, $H_{c,\perp}$ also increases, $\Delta\theta_{50}$ decreases from 13° to 10°, but $M_{s,\perp}$ remains unaffected. The benefits of the positive, moderately high bias voltage in significantly improving $H_{c,\perp}$, $M_{r,\perp}/M_{s,\perp}$, and $\Delta\theta_{50}$ are attributed to the improved *c*-axis orientation, as evidenced by the lowered values of $\Delta\theta_{50}$. Also worth mentioning is the observation that films deposited on polyimide at 0–400 V bias show coarse grains and no clear columnar structure. Only at higher bias voltages of 1200 and 1500 V does columnar grain structure appear. It is important to realize that, in applying a positive bias, more secondary electrons will be attracted to the substrate, thereby inducing more heating, which may account for some of the magnetic property and microstructure changes. According to Suzuki *et al.* [74], however, induced substrate heating is not the main cause of their observed changes in the grain structure and magnetic properties.

The incidence angle of coating flux is known to affect sputtering yield [63], surface morphology [89], grain structure [90], internal stress [63], and other properties of sputter-deposited films. The effect of the incidence angle is particularly important in the case of ion-beam sputtering. Feuerstein and Mayr [91] equipped the sputtering cathode with adjustable shieldings to change the maximum incidence angle of depositing atoms arriving at the substrate. Oblique incidence at larger angles was observed, which created longitudinal components because of self-shadowing of the growing film. In a later study using large-scale roll-coating systems, Mayr *et al.* [69] reported that decreasing incidence angle resulted in better parallel alignment of columns and higher values of the anisotropy field, H_K. Niimura *et al.* [70] used their FTS system to study the incidence-angle effect on the *c*-axis orientation in Co–21 at % Cr films deposited on glass substrates. A special mask had to be installed to collect only sputtered atoms with "quasi-coherent incidence" to the substrate so that the effect of the incidence angle could be more clearly evaluated. At low argon pressures (40 to 106.6 mPa), the effect of the incidence angle is unimportant, thereby allowing sharp *c*-axis orientation to be obtained below 45° incidence angle. This result was taken to imply that surface diffusion might be more dominant and that the physical layout of the substrate with respect to the dual target in the plasma-free FTS system with low working gas pressure offers good flexibility for preparing sharp *c*-axis orientation in the Co–Cr films.

4.2. Physical vapour deposition by evaporation

The deposition rate of the evaporation process can be made many times higher than that by sputtering. This advantage loomed big in the early years of the PMA-film development when the rate was limited to only 0.2–0.3 nm s^{-1}. In 1981, Sugita *et al.* [92–95]; Honda *et al.* [96] and Yoshida *et al.* [97] launched a series of studies to develop this process for the fabrication of Co–Cr PMA films. Using an electron beam whose power could go up to 16 kW, they initially attained a maximum deposition rate of 600 nm s^{-1} (or 2.16 mm h^{-1}). In 1987 [94], a continuous evaporation-coating process was developed which reached a remarkably high deposition rate of 1000 nm s^{-1} (or 3.6 mm h^{-1}). This rate is comparable to those observed in the production of conventional particulate tapes. It will be discussed later that such high rates, however, have some adverse effects on the microstructure and magnetic properties of the films.

Another advantage of the evaporation process over sputtering is the simplicity of the deposition equipment required. As a case in point, Fig. 8 shows a system for continuous coating of tape substrates by evaporation. In comparison with the sputtering equipment shown in Fig. 6 for similar substrates, the system for evaporation deposition is distinctly simpler. Brucker *et al.* [98] described another system for plasma-enhanced single- or co-evaporation deposition that also has simple design features. In terms of economy, simple equipment means lower initial cost and easier operation, both of which would enhance the practical value of the PMR technology. This economic advantage, coupled with the fact that Co–Cr films prepared by evaporation deposition display comparably good properties for PMR applications, should help promote this process.

The PMR performance of evaporation-deposited films was assessed by Sugita *et al.* [95]. Using a ferrite-ring head for characterizing the recording, the latter media showed reasonably good magnetic properties: $H_K = 1.59 \times 10^2$–3.58×10^2 kA m^{-1}, $H_{c,\perp} = 3.98 \times 10^4$–$5.57 \times 10^4$ A m^{-1}, $M_s = 300$–600 e.m.u. cm^{-3}.

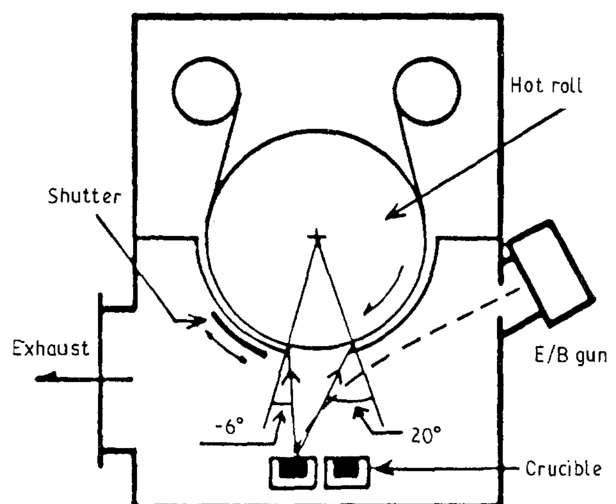

Figure 8 Sketch of continuous roll coater.

For film thickness in excess of 0.2 μm, high reproduction voltage and high carrier-to-noise ratio at linear density over 3937 kFRPM were recorded.

All Co–Cr films prepared by evaporation deposition at rates in excess of 200 $nm\,s^{-1}$ display the [0001] texture and PMA provided M_s falls below 350 e.m.u. cm^{-3} [92]. However, the best value of $\Delta\theta_{50}$ is 7°, which, though matching many sputtering results quite well, is 5° greater than the best value attained in sputtering [82, 97].

In the work by Sugita and others, the evaporation source is one of the Co–Cr alloys of a predetermined composition. Honda and Storer [99] observed a gradual increase in M_s with the deposition time. They attributed this increase to a loss of Cr from the molten alloy source because of the higher vapour pressure of Cr than that of Co. The differential evaporation rates of Co and Cr were later confirmed by Brucker *et al.* [98]. The progressive exhaustion of Cr results in a composition gradient along the film thickness.

To solve the problem of Cr loss in the single source, Pronk and Lodder [100] tried co-evaporation using separate sources of cobalt and chromium. At an intermediate incidence angle, $\alpha_i = 30°$, where α_i is the angle deviating from normal incidence, the (0001) plane and the magnetic anisotropy axis were found to tilt toward the Co source. Despite this tilt, the films show good perpendicular magnetic behaviour for PMR. Also at low deposition temperatures, relatively high coercivities were measured, which was ascribed to a segregation of Cr caused by the shadowing effect during deposition.

In one study, Honda *et al.* [96] concentrated on the effect of deposition rate and found that decreasing the rate would increase perpendicular coercivity and segregation of Cr. They concluded that, because of the vast difference in the deposition rate, much higher T_s (250 °C versus 125 °C) is required for the same high $H_{c,\perp}$ for evaporation-deposited than for sputtered films.

The effect of T_s on the magnetic properties and microstructure of the evaporation-deposited films was studied by Honda and Storer [99], who also examined the role played by argon-ion bombardment and post-deposition annealing. Again 250 °C seems to be the optimal substrate temperature at which perpendicular coercivity, $H_{c,\perp}$, and anisotropy field, H_K, show maximum values, alignment of the *c*-axis is sharper, and grain size is smallest. Ion bombardment tends to decrease M_s and to change the sign of the internal stress from tensile to compressive. When $T_s < 150$ °C, H_K decreases due to ion bombardment. Deposition at temperatures below 200 °C followed by annealing around 300 °C (or above 400 °C in high vacuum) would increase (or decrease) M_s. A decrease in M_s and increases in H_K and $H_{c,\perp}$ are the results of annealing at 400 °C.

Brucker *et al.* [98] introduced a novel evaporation-deposition process in which an RF coil between the source and substrate was operated at 200 W to generate a plasma. The plasma was sustained by the metal evaporant without a carrier gas. To avoid Cr deficiency in the film resulting from different evaporation rates of Co and Cr in the single source, co-evaporation of separate sources of the two elements at an incidence angle ~ 30° was used. The Co–Cr films prepared by the plasma-enhanced evaporation-deposition process displayed increased perpendicular coercivity with the substrate temperature somewhat lowered to the range 20–250 °C. This novel technique allows use of lower-temperature, cheaper polymer tapes as substrates, thus improving the economy of the process.

Despite the limited number of studies thus far conducted on evaporation deposition, its applicability to fabricating PMA films is well established. Also clearly demonstrated are the higher deposition rate, lower initial cost of equipment, and possibly less expensive operation. Whether or not these advantages are sufficient to give the evaporation process a clear edge over the sputtering process for industrial production remains to be seen. The problem of the evaporation process is two-fold. Inherently, it has the problem of maintaining the original composition of the alloy in the single-source approach with two different evaporation rates. When co-evaporation is adopted in place of the single source, qualities of the film such as the *c*-axis texture and composition homogeneity [100] could suffer. Moreover, the deposition rate of the sputtering process has been increased considerably by using the special techniques mentioned. Consequently, the evaporation process may have lost its main competitive edge over the sputtering process. Recently, however, Hitachi workers [97] applied the *e*-beam co-evaporation process to fabricating Co–Cr films on 50 μm thick polyimide tape at rates up to 600 $nm\,s^{-1}$ (or 2.16 $cm\,h^{-1}$) in the continuous roll coater shown in Fig. 8. To improve the [0001] texture and magnetic properties of the film, the roll was heated to 160–265 °C and the tape was precoated with 30 nm of Ge. This is a case close to mass-production methods of the evaporation-deposition process for PMR media.

4.3. Electroless deposition

Researchers at NEC Laboratories and Waseda University in Japan worked together on the electroless plating process [101–104]. The thrust of applying this process to the Co–alloys is the production of rigid discs with PMA films. Rigid discs have distinct advantages over tapes as PMR media, notably higher wear resistance and greater ease of handling. In practice, this means that PMR discs would show better productivity and higher reliability in storing and retrieving the information. The electroless plating is also capable of uniform coating over substrates with nonplanar surfaces. Hence, it is an effective technique for fabricating perpendicular heads for PMR.

The practicality of this process hinges on whether or not an efficient plating bath can be found for the desired film composition. Through a series of experiments, Koiwa *et al.* [103] developed baths that produced films showing "excellent" PMR capability. Initially, Co–Ni–P in the deposit was found to increase the anisotropy field markedly [103]. Ito *et al.* [105] discovered that Re can also improve the

Co–Ni–P films by decreasing the saturation magnetization, thereby allowing attainment of the optimal PMA properties. Consequently, Osaka *et al.* [102] used an ammoniacal malonate-tartrate-succinate electrolyte to produce Co–Ni–Mn–Re–P films on aluminium-alloy disc substrate, the surface of which had been precoated with a Ni–P film by electroless plating. The plating bath has the following complex composition in mole liter^{-1}: $CoSO_4$–0.06, $NiSO_4$–0.06 to 0.16, $MnSO_4$–0.05, NH_4ReO_4–0.05, NH_4ReO_4–0.005, NaH_2PO_2–0.30, $(NH_4)_2SO_4$–0.50, sodium malonate–0.30, sodium tartarate–0.20, sodium succinate–0.30. The bath has a pH value of 9.2 and a constant temperature of 80 °C. The films display anisotropy energy of 9.5 to 2.2×10^{-2} J cm^{-3}, perpendicular coercivity of 3.5×10^4–1.01×10^5 A m^{-1}, and saturation magnetization of 104 to 252 e.m.u. cm^{-3}. The PMR performance of disc media with 0.5 μm thick PMA films and 0.33 μm gap length was evaluated by Winchester heads at 0.2 μm head-medium spacing. "Excellent" results were obtained: linear recording density (D_{50}) 2008–2126 kFRPM, signal-to-noise (SNR) 26 dB, overwrite characteristics − 30 dB. Moreover, higher recording density was obtained at 2667 kFRPM by decreasing the film thickness from 0.5 μm to 0.2 μm and the head-medium gap from 0.33 μm to 0.12 μm.

The same team later modified the bath by eliminating $MnSO_4$ so that Mn would be absent in the plated film [103]. Specific compositions of the latter films are given as a function of the concentration of sodium malonate in Table II. Note that an increase in the concentration of sodium malonate affects the concentrations of Co and Ni in opposite directions. The change in concentration of sodium malonate was also seen to affect the perpendicular coercivity and other magnetic properties of the films having thickness < 5 μm.

4.4. Electrodeposition with or without anodic oxidation

Chen and Cavallotti [8, 106] succeeded in applying the electroplating process to preparing PMA films of cobalt. Their work is especially interesting for two reasons. First, as far as can be found in the literature, this is the only case in which electroplating is used to prepare the PMA films without involving aluminium substrates and anodic oxidation. Second, they were able to develop the PMA in pure cobalt, signifying that the condition $H_{K,\perp} > 4\pi M_s$ for PMA proposed by Iwasaki and Ouchi [36] is not critical, as was later reconfirmed by Hoffman *et al.* [107]. The plated films contain nonmagnetic $Co(OH)_2$ precipitates that separate the Co particles in the matrix. Therefore, the origin of PMA in the film could be a combined effect of crystalline and shape anisotropy of the cobalt particles. By adjustment of current density, bath temperature, and bath concentration, the demagnetizing field, H_d, and the perpendicular coercivity could be optimized by control of interparticle separation.

The plating bath used by Chen and Cavallotti consists of one molar Co–sulphamate, an anode depolarizing reagent and buffer; its pH value varied between 6.4 and 6.5. X-ray diffraction analysis on the films revealed that sharp [0001] texture was developed in a range of current density showing a dispersion of $\Delta\theta_{50} = 9$–$10°$. To further improve the magnetic properties, the films were subjected to an anodizing treatment in an etching bath composed of an acid solution of sulphuric acid and thiorea. The film is placed in the anode of the etching cell, and the anodizing time is critical. An increase in etching time significantly increases the coercivity field, H_c, and the M_r/M_s ratio but decreases H_d and H_s where $H_s \simeq H_c + H_d$ is the saturation field [106]. The PMR performance of the PMA Co films was not reported.

As early as 1975 (two years before the first preparation of Co–Cr PMA films for high-density magnetic recording by Iwasaki and Nakamura [3]), Kawai and Ueda [108] electrodeposited Co into the micropores of anodic oxide films on aluminium. The films showed remarkable PMA and other attractive magnetic properties (e.g., $H_c = 3.98 \times 10^4$–7.96×10^4 A m^{-1}), which the authors modestly but correctly suggested as having "potential applications for high bit density memories and recording." This approach of combining anodic oxidation of aluminium substrates and electrodeposition of a ferromagnetic metal into the micropores of the alumite to develop PMA, however, was not further pursued until 1985, when Shiraki *et al.* [9] used essentially the same two major processes but inserted an additional process in order to enlarge the micropore for reducing the coercivity to the $< 7.96 \times 10^4$ A m^{-1} level required for PMR.

As in the case of electroless plating, the combined application of anodic oxidation and electrodeposition to fabricating PMA films was undertaken by a team of workers at a university and an industrial laboratory in Japan [9, 109, 110]. Another similarity between these two cases is the advantage that rigid discs can be prepared at high productivity with better reliability and easy handling. However, the present procedure is much more complex as evidenced by the eight-step procedure depicted later. Also worth noting is the difference that the ferromagnetic material is no longer a Co–Cr alloy, but a transition metal (Fe, Co, or Ni).

The principles underlying the present procedure are the creation of a cellular structure of sesqueoxide, Al_2O_3, on the surface of an aluminium plate (Fig. 9b) and the electrodeposition of a ferromagnetic metal into the micropore of each oxide cell. When the procedure is properly done, the deposited ferromagnet

TABLE II Film compositions as a function of sodium malonate concentration

Concentration of sodium malonate (mol l^{-1})	Composition of films, at %			
	Co	Ni	Re	P
0.30	17.9	64.6	5.8	11.7
0.50	20.2	62.1	5.6	12.1
0.75	25.8	57.3	5.8	11.7

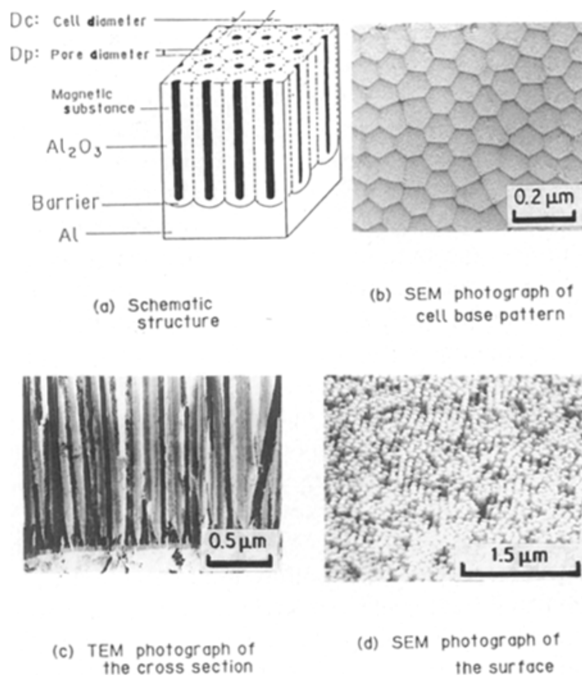

Figure 9 Structure of the magnetic alumite disc.

is a single crystal in column or needle form (Fig. 9a, c, and d) with the easy axis of magnetization oriented in the direction normal to the film plane. With the pore size enlarged to 40 nm from 20 nm, the deposited columns display strong PMA as well as perpendicular coercivity at the desired level for PMR. From the combined results of several workers, a composite procedure of the process may be listed as follows:

1. *Selection of substrate material*: the substrate material is Al–4 wt % Mg. The base-metal aluminium must be 99.99% pure; otherwise, the cell structure of the subsequently formed Al_2O_3 in Step 3 would not be sufficiently regular [109]. The addition of 4% Mg is to ensure a good finish of the substrate surface [109].

2. *Preparation of substrate surface*: first by diamond turning, then etching in an alkali solution containing 0.5% NaOH at 20–70 °C.

3. *Barrier-layer formation*: a dense layer is formed on the surface prior to anodic oxidation in 1% phosphoric acid. This layer is electronically conductive and is formed to ensure a uniform deposition of Fe, Co, or Ni in Step 6 [110].

4. *Anodic oxidation*: in 3% oxalic acid bath [9] or in a sulphuric-acid, nitrogen-bubbled bath [110] at 20–30 °C.

5. *Pore enlargement*: to increase the average diameter of the micropores from the usual 20 nm, the oxidized substrate plate is immersed in 1% phosphoric acid plus 5% NH_2SO_2OH solution at 20–40 °C [110]. This process also tends to increase the porosity in the alumite, thus allowing more ferromagnetic deposits to be made for higher magnetic flux density [110]. For perpendicular coercivity below the 7.96×10^4 A m^{-1} required for PMR, the desired pore diameter is > 40 nm [9, 110].

6. *Electrodeposition of Fe, Co, or Ni*: use a plating bath containing 0.1–1.0 mol l^{-1} sulphate with the chosen cations at a pH value of 4 to 5 [110]. This step continues until the pores are completely filled.

7. *Buff polishing*: by silica-sol for a few minutes. The final surface finish of the alumite layer, measured in terms of peak-to-valley height, should be less than 100 nm.

8. *Surface coating*: sputter-deposit 20 nm of SiO_2 to form a surface film for protection against mishandling and corrosion.

This procedure is summarized in Fig. 10.

X-ray examination showed that the Fe deposits in the pores are in the form of needles, each of which is a single crystal with the [1 1 0] growth direction. Hysteresis and Mössbauer measurements revealed the presence of strong PMA in the direction normal to the film plane [9]. The dependence of $H_{c,\perp}$ on the cell and pore diameters was studied in detail; the results are shown in Figs 11 and 12. For Co and Fe, $H_{c,\perp}$ decreases as pore diameter increases, whereas films containing Ni, $H_{c,\perp}$ show a maximum at a pore diameter of ~ 40 nm. $H_{c,\perp}$ is independent of the cell diameter, however. Rigid discs with the PMA deposits prepared by the anodic oxidation method were claimed to exhibit "excellent" feasibility for high density (up to 24 k bytes cm^{-1}) [1 1 0] recording. The media exhibit stability in corrosion tests at 40 °C under 90% relative humidity for over 1000 h and excellent wear resistance over 5 million head passes [110]. More recently, the same workers refined the procedure outlined above (using 99.999% Al to coat 50 μm thick PET substrates with (1 1 1) preferred orientation by sputtering) so that the method could be applied to the polymer substrates for making flexible

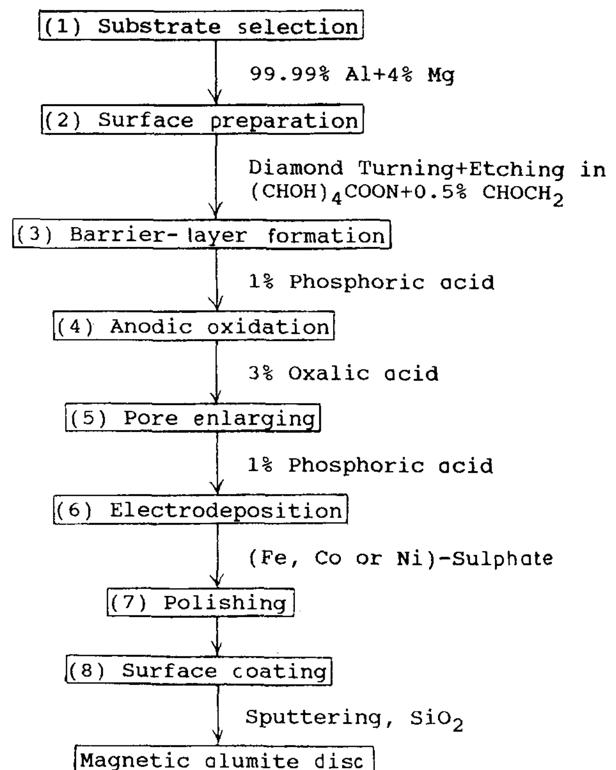

Figure 10 Block diagram of the 8-step procedure for the preparation of perpendicular magnetic media by the anodic-oxidation method.

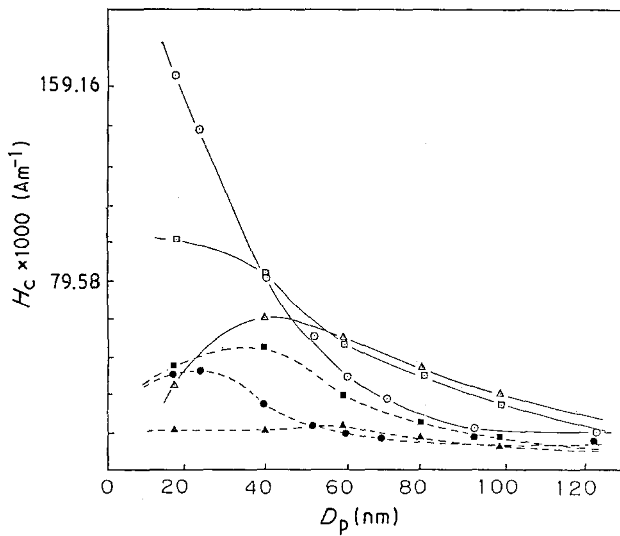

Figure 11 Pore-diameter dependence of the perpendicular (⊥) (●) Fe; (▲) Ni; (■) Co and parallel (‖) (○) Fe; (△) Ni; (□) Co coercivity.

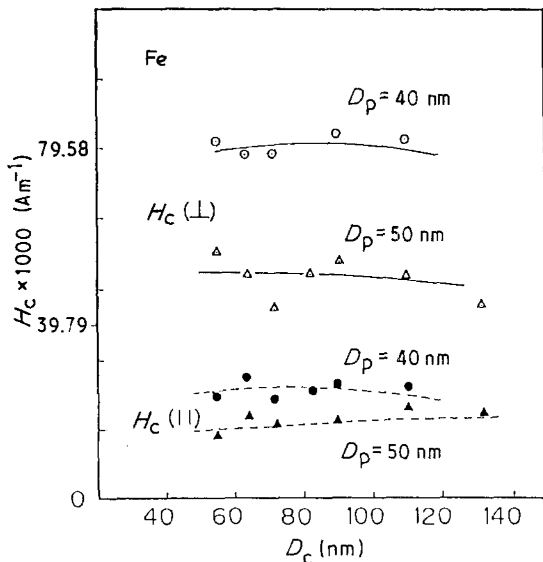

Figure 12 Cell-diameter dependence of the perpendicular (⊥) and parallel (‖) coercivity.

PMR discs [111]. The latter media were claimed to display high quality for PMR performance.

5. Characterization of PMA films
5.1. Microstructure
5.1.1. Phase identification
For the sake of completeness, it should be mentioned that Ohkoshi *et al.* [112] examined the separation of phases in the PMA films of Fe–Cr alloys. To understand the possible variation of phases in the Co–Cr films, we need to examine the phase diagram of this alloy system. Several versions have emerged in the literature, of which the one proposed by Allibert *et al.* [113] is now considered [114, 115] the most reliable [115]. It is reproduced in Fig. 13, which shows that, at (17–23) at % Cr, the alloys exist below the solidus curve in a single-phase γ of the fcc crystal structure. At lower temperatures, the γ-phase is transformed into another phase ε of the hcp structure. The γ + ε two-

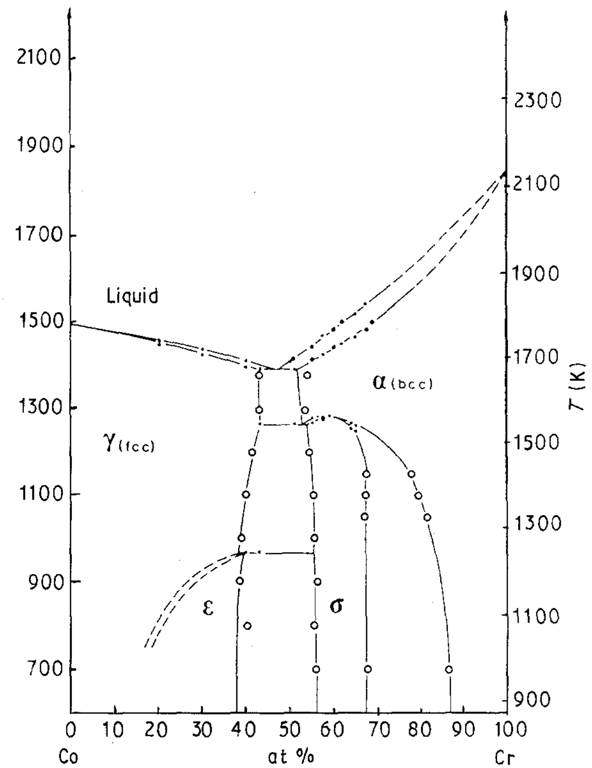

Figure 13 Experimental phase diagram proposed for the Co–Cr binary system by Allibert *et al.* [113].

phase region is very narrow (~ 40 °C). Although the low-temperature phase is universally called ε, the high-temperature phase is designated as γ in Fig. 13, as α by Hansen [116] and the ASM Handbook [117], and as β by Matsunaga [118]. The lattice parameters of the hcp ε-phase are $a = 0.2515$ nm and $c = 0.4053$ nm for the Co–16.7 at % Cr alloy [119]. The phase-diagram features of the Co–Cr system coupled with the tendency of PVD-processed films to exist in a metastable state promote the single ε-phase in the PMA films. While this favoured phase indeed prevails in most cases, Smits *et al.* [115] detected a composition shift in the Co–(17–23) at % Cr films prepared by ion-beam sputtering. Specifically, they detected a depletion of Cr in local regions, where a nonmagnetic phase emerged. Evidence of the composition shift is seen in the grain refinement induced at high T_s and the higher values of M_s and K_u for the films than for the bulk alloys. Similar results were also reported by Iwasaki and Ouchi [36] and others [120–122]. The nonmagnetic phase was identified as not being the intermediate (56–62 at % Cr), tetragonal σ-phase, as might have been deduced from the phase diagram shown by Hansen [116]. Rather, it was identified as the Cr oxide, whose formation was related to the high affinity of Cr for oxygen.

Maro *et al.* [123] conducted an interesting study in which Co–(17–20) at % Cr was co-evaporated and deposited with polyethylene (PE) on heated (to 200 °C) polyimide substrates. Their original objective was to improve the flexibility of the film by filling the space between columns with the polymer. The Co–Cr + (34–55)% PE films turned out to be amorphous. Also the amorphous films display soft, instead of hard,

magnetic behaviour first, followed by superparamagnetism with increasing PE content. These polymer-incorporated films may find applications other than PMR.

5.1.2. Composition inhomogeneity

Several workers investigated the problem of composition inhomogeneity in the sputtered films of Co and Cr. Maeda and Asahi [124], Masuya and Awano [120], and Maeda and Takahashi [125] observed similar results. When well developed, the films consists of grains, each of which has a Cr–rich core surrounded by a Co–rich ring. The grain structure of the film also features Cr–enrichment at the grain boundaries. Moreover, the segregation of Co and Cr in the grains leads to the formation of chrysanthemum-like patterns (CPs) [124]. Masuya and Awano [120] related the compositional segregation to two major sputtering parameters: argon gas pressure P_{Ar}, and substrate temperature, T_s. Valuable information was obtained by following the development sequence of the segregated microstructure. In the investigation, only one of the parameters was changed as follows: $T_s = 90$, 140, and 160 °C with P_{Ar} fixed at 0.533 Pa; and $P_{Ar} = 0.533$, 1.333, and 3.999 Pa with T_s kept at 140 °C. The observed changes in microstructure are shown in Figs 14 and 15. Even for T_s as low as 90 °C, segregation is evident due to the formation of Cr–rich regions (appearing after etching as the dark images shown in Fig. 14a) at the grain boundaries. At $T_s = 140$ °C, the Cr–rich region is surrounded by a Co–rich region (appearing as the bright image) in the centre of each grain (Fig. 14b). Also observed are small isolated Co–rich regions dispersed within the grain. Fig. 14c shows the additional features of Co–rich regions in the form of chrysanthemum flower petals radially emanated from the Co–rich rim around the Cr–rich region in the grain centre. This series of TEM micrographs clearly shows that the degree of segregation increases with increasing T_s. The effect of P_{Ar} on compositional segregation is shown in Fig. 15. Note the marked similarity of the CP microstructures in Figs. 14c and 15b, implying that the largest degree of segregation occurred at an intermediate (1.333 Pa) value of P_{Ar}. Significant increases in M_s and H_c were detected accompanying the changes in microstructure caused by compositional segregation.

In a theoretical analysis, Andra and Danan [126] adopted the simple assumption that segregation of Cr at the grain boundaries either forms the main obstacles in the Co–Cr films to domain wall-motion or causes a breakdown of the exchange coupling between neighbouring grains. Either effect is thought to contribute to the increase in perpendicular coercivity that has been widely observed in the Co–Cr films [125]. The analysis results favour the wall-displacement model for exchange-coupled grains over the rotational-magnetization model for exchange-isolated columns. In view of the results of Masuya and Awano [120], however, the analysis by Andra and Danan [126] may be critized for focusing on the segregation of Cr (Fig. 14a) in the early stage. In reality, the phenomenon yields both Cr– and Co–rich regions within grains; together, they form the spectacular flower patterns. Therefore, a more complete analysis would necessitate the inclusion of other segregation phenomena observed in Figs. 14b, c, and 15.

5.1.3. Grain structure and columnar growth

Many studies were conducted on the microstructure of the PMA films of Co–Cr by applying TEM and selected-area diffraction (SAD) or convergent-beam electron diffraction (CBED). By combining the results of various workers, the sequence of the development of the final microstructure may be summarized as follows: when an amorphous substrate (e.g., polymer or

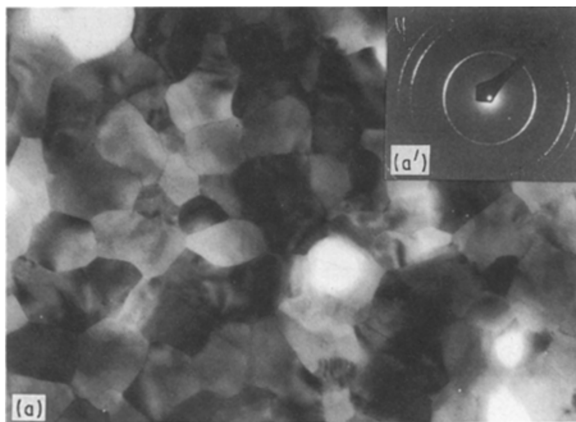

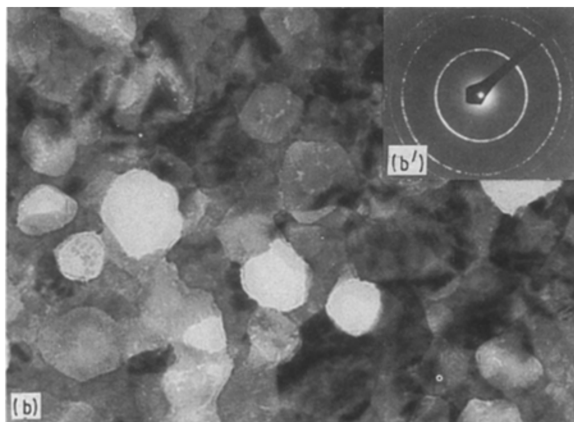

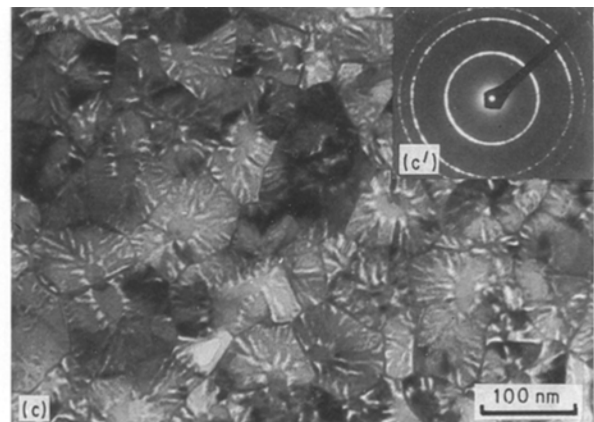

Figure 14 Segregated microstructures in Co–Cr films deposited at a P_{Ar} of 0.5332 Pa and T_s adjusted to (a) 90, (b) 140, and (c) 160 °C.

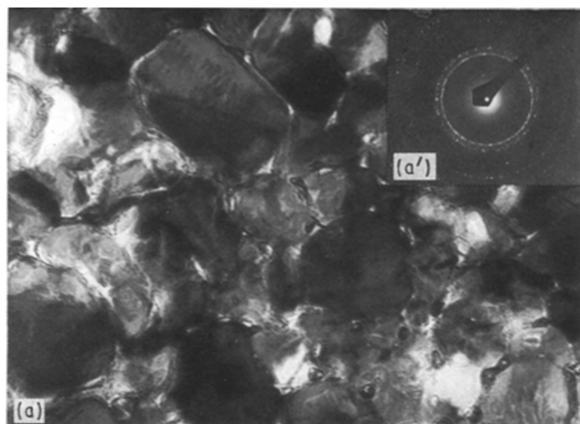

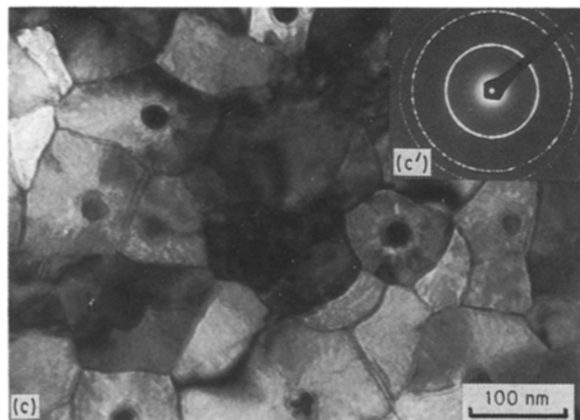

Figure 15 Segregated microstructures in Co–Cr films deposited at a T_s of 140 °C and P_{Ar} adjusted to (a) 3.999, (b) 1.333, and (c) 0.5332 Pa.

glass) is used, the films are initially amorphous, as evidenced by a broad halo in the SAD pattern [127]. After film thickness exceeds roughly 5 nm, CBED patterns show sharp crystalline Co–Cr reflections, signifying the formation of randomly-oriented crystallites in the amorphous matrix [127]. As deposition continues, additional crystallites are nucleated and existing crystallites grow, eventually converting the entire matrix to crystalline [127]. After the film thickens to > 100 nm, columnar growth with [0001] preferred orientation dominates, leading to the final *c*-axis texture. This sequence of events explains why all Co–Cr films that do not have heavy doping of a polymer [123] are crystalline with preferred orientation. The state of the initial deposit on a crystalline substrate, whether amorphous or crystalline, has not been critically examined.

The predominant feature of the microstructure of a well-developed Co–Cr film is the columnar growth in straight cylindrical, conical, or a mixture of the two shapes [127]. Equiaxed [122, 127] and elongated grains [127] are also observed in the plane image of the microstructure. The formation and salient features of the columnar structure depend strongly on the sputter-deposition conditions, notably the gas pressure of the argon and the substrate bias voltage. The influences of the latter two conditions are well summed up by Honda and Storer [128]: the columnar structure generally appears in sputtered films on a zero-biased substrate in high P_{Ar}. Columns become finer and eventually disappear as argon pressure is lowered [129] or bias voltage is increased [130].

Defects observed in the microstructure by various workers include: microvoids at grain and columnar boundaries [131]; microtwins in the direction normal to the axis of the columnar grains [131]; stacking faults; nodular defects [132]. Glocker *et al.* [133] conducted a detailed study of void formation in the Co–20 at % Cr films that were prepared under these conditions: RF-sputtering, silicon substrates with temperature varying from 25 to 200 °C, and argon pressure of 0.533 or 2.133 Pa. In all four cases from which the results were reported, voids of sizes varying from 15 nm to 130 nm were detected at the bottom of the 1 μm thick films; however, only in one case were voids observed for 200 nm in diameter at the top of the films. Their results imply that voids are more likely formed in the initial amorphous deposit. Yoichi *et al.* [134] observed stacking faults of the (0002) plane in the hcp phase but detected neither a nonmagnetic secondary phase nor voids in the Co–Cr films evaporation-deposited on heat-resistant polymer substrates coated with Ti underlayers.

Glocker *et al.* [133] also examined grain-size variation with film thickness. Their results indicate that grain size, *d*, is always larger at the top of the film than at the bottom and that the increase in *d* over a film thickness, $t_f = 1$ μm amounts to a factor of 2.8–7.3. The relationship between *d* and t_f is more systematically studied by Lodder *et al.* [61], whose results are shown in Fig. 16. The grain size increases almost linearly with the film thickness. The latter authors proposed that the mechanism of grain growth is a statistical variation in the local flux of the depositing atoms at the individual grains, but it may also be promoted by the driving force of lowering the grain-boundary energy. The phenomenon of nodular defect formation has long been investigated in sputtered films of many materials [135–138]. Artley *et al.* [132] have recently studied this phenomenon in Co–Cr films deposited on polymer substrates. They concluded that the nodules are nucleated mainly at the metal/substrate interface, but not by dust or contaminants introduced by mishandling (e.g., fingerprints leaving non-volatile oil on the substrate surface). For the polyimide substrate, the nucleation of nodules is

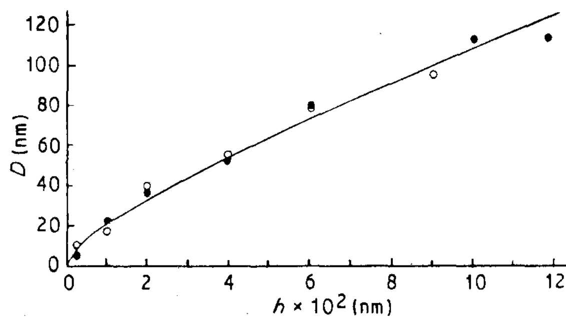

Figure 16 Crystal size D as a function of the layer thickness h: (●) = multitarget; (○) = alloyed target.

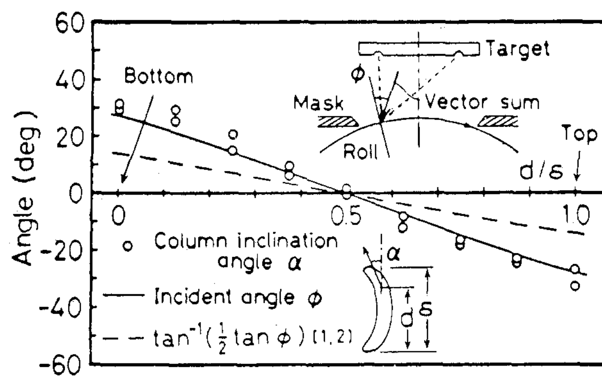

Figure 17 Relationship between column inclination and mean incident angle [144].

related to an exudate of the polymer. The exudate is identified with the residual of a special solvent, n–methyl–1,2–pyrrolidone(H_3C–($NCOCH_2CH_2CH_2$)), used by the polyimide manufacturer. The solvent leaves small amounts of residue over many spots on the substrate surface. The residue is non-volatile, but soluble and diffusible, and therefore capable of nucleating nodular growth at the interface. After switching the substrate polymer to 'Stabar' polyether–ether–ketone (PEEK), the nodule formation was greatly suppressed (100–200 nodules cm^{-2} for films deposited on PEEK substrates versus 1000 nodules cm^{-2} for films deposited on polyimide). With suppressed formation of nodules, the PMA films will have smoother surface (R_A = 1–2.5 nm), thus improving wear resistance and upgrading the recording performance of the media. Another advantage of the PEEK polymer substrates is that degassing is not required.

Sputtered Co–Cr films are expected to show surface morphology featuring a honeycomb-like network with slightly protruding dome-shaped tops. This kind of topography is the natural consequence of the columnar growth. The size and depth of the protrusion of domed tops may be considerably enhanced wherever nodular defects are formed during columnar growth. The degree and scope of this enhancement depend largely upon the origin of the nodular defects. When the formation of nodular defects is pronounced, the film surface will have a cauliflower appearance.

Films deposited on continuously transported substrates using such techniques as the roll-magnetron-sputtering process [77, 83] show special morphology. Since the latter process has great application potential for mass production, morphology of the extended films has been actively investigated. Columns in the Co–Cr films prepared by the evaporation process onto a moving substrate are bowed in the direction of the substrate motion. The bowing is attributed to the variation of the incidence angle when the substrate is moving over a roll during deposition [139]. Originally the column bowing is described by a tangent rule [140, 141], which states that the inclination angle, α, of the bowed columns defined in Fig. 17 is related to the mean incidence angle, ϕ, by the expression

$$\alpha = \tan^{-1}(1/2 \tan\phi)$$

where ϕ is the angle between $\boldsymbol{n}$ (normal vector to the film surface) and $\boldsymbol{v} = \boldsymbol{v}_1 + \boldsymbol{v}_2$, with $\boldsymbol{v}_1$ and $\boldsymbol{v}_2$ being the atom-beam vectors drawn from each line source to the deposition point on a substrate. Also found is the canting of the c-axis with respect to the film normal of deposits on a moving substrate resulting from the effect of the incidence angle [142, 143]. Tanaka *et al.* [144] observed elongation of grains in the surface layer of the continuously-deposited film along the substrate moving direction. The grain elongation is thought to be due more to variation in incidence angle during deposition than to oblique incidence. Also found is the relation that the column inclination angle, α, corresponds more closely to the mean incidence angle, ϕ, than to the angle, $\tan^{-1}$ (1/2 tanϕ), given by tangent rule.

An important feature of the microstructure of PMA films is of course the formation of the (0 0 0 1) texture. The mechanisms of nucleation and growth of grains or columns leading to the formation of the texture have been studied. According to Lodder *et al.* [61], the nuclei of grains with the preferred orientation originate from the tendency of the sputtered atoms of the Co–Cr alloy to condense on the most densely packed crystal plane, (0 0 0 2) of the h c p structure, parallel to the substrate. Upon growing, the preferred orientation is maintained because it is also the fastest-growing crystallographic direction. Van der Drift [145] has shown, in his "survival of the fastest" growth model, that crystallites with the fastest-growing axis survive while growth of other oriented crystallites is suppressed. For the Co–Cr films, the fastest-growing axis is oriented normal to the substrate plane. Glocker *et al.* [133] later extended the argument by applying Drift's model to the case in which amorphous substrates, such as glass, are used. However, they emphasize that the mobility of adatoms on the growing surface must be sufficiently high; otherwise, low adatom mobility leads to poor c-axis orientation and weak perpendicular anisotropy.

Niimura *et al.* [146] studied the dependence of the c-axis dispersion in terms of $\Delta\theta_{50}$ on the film thickness, t_f, using either the FTS apparatus or the conventional d.c.-planar-magnetron sputtering process (DCPMS). The films prepared by DCPMS show considerable increase in $\Delta\theta_{50}$ with decreasing $t_f < 400$ nm. This $\Delta\theta_{50}$ increase is attributed to the bombardment of electrons ejected from the central area of the single target, where the magnetic field is not

strong enough to confine the electrons. Films prepared by FTS, however, showed insignificant dependence of $\Delta\theta_{50}$ on t_f, and $\Delta\theta_{50}$ was less than 5 ° even at t_f = 20 nm. They considered this as another attraction of the FTS technique.

The effect of the underlayer on the preferred growth of the *c*-axis in the Co–Cr films was evaluated. Because polymers such as polyimide and polyethylene terephthalate (PET) are amorphous, it is reasonable to assume that inserting a crystalline underlayer, especially those having the right (h c p or possibly f c c) crystal structure, should help promote nucleation and growth of the (0 0 0 1) orientation. Indeed, this was confirmed in h c p Ti underlayers by Gill and Rosenblum [147] and Yoichi *et al.* [134], in h c p Ta underlayers by Gill and Yamashita [148]. In their first study, Gill and Rosenblum [147] sputter-deposited Co–Cr on either b c c Cr or h c p Ti underlayers. The perpendicular anisotropy of the film deposited on Cr was poorer than that deposited on h c p Ti. In the second study, Gill and Yamashita [148] used the ion-beam technique to sputter-deposit Co–18 at % Cr on Ta underlayers in either b c c or h c p structure. Again the h c p Ta underlayer produced columnar grain structure and the preferred orientation very early, whereas films deposited on the b c c Ta underlayers show more random orientation. The (0 0 0 1) X-ray half-width for Co–Cr on h c p and b c c Ta were 8 ° and 14 °, respectively. Also films deposited on the b c c Ta underlayer display larger in-plane coercivity. A less favourable effect of the permalloy underlayer on the formation of the [0 0 0 1] texture was reported by Tomie *et al.* [149]. While Co–Cr films deposited directly on PET substrates had a sharp distribution of the *c*-axes of individual crystallites, the presence of the permalloy underlayer caused considerable scattering of the *c*-axes. As to the mechanism of the underlayer effect, the latter authors noted that the h c p Ta itself has a highly-preferred *c*-axis orientation of grains. Therefore, they considered epitaxial growth of Co–Cr grains on the h c p Ta underlayer as a possibility.

Overemphasizing the importance of using h c p underlayers to promote the *c*-axis texture in the Co–Cr films is unnecessary, however. The *c*-axis texture has been observed in Co–Cr films deposited on other crystalline-substrate materials such as f c c Ni–Fe having (1 1 1) texture [150], orthorhombic sapphire, and (1 1 1) single crystals of cubic silicon. Even more intriguing is the fact that a number of amorphous underlayers or substrates such as Ge [151, 152], glass, Ta–W–Ni, polyimide, and PET have proven effective in developing the *c*-axis orientation in the Co–Cr films. The role played by the amorphous Ge underlayer was evaluated by Futamoto *et al.* [151] and by Schrauwen *et al.* [152]. Applying the *e*-beam evaporation method, Futamoto *et al.* first coated polyimide substrates with a wide variety of elements (Al, Si, Sc, Ti, V, Cr, Ni, Ge, Y, Zr, Nb, Ru, Rh, Pd, Sn, Sb, Hf, Re, Pt, and Bi) and oxides (SiO_2, MgO, Al_2O_3, TiO, and ZnO) to 30 nm thickness at 180 °C. Four underlayer materials, Sc, Ti, Si, and Ge, are found to be effective in improving the *c*-axis orientation, whereas the other materials tend to increase $\Delta\theta_{50}$. Fig. 18 compares the cross-sectional TEM micrographs of Co–Cr films deposited on polyimide substrates and on Ti and Ge underlayers. The micrographs clearly show that amorphous Ge is particularly effective in preparing highly-oriented Co–Cr films; pillar-like crystals are grown vertically through the entire film thickness. The latter films display strong PMA and markedly improved read-write characteristics with very high

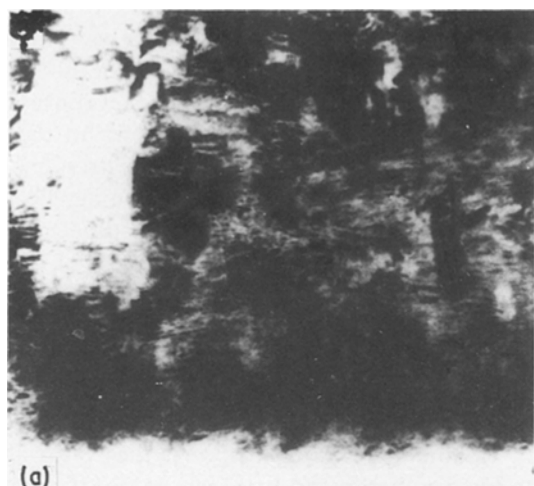

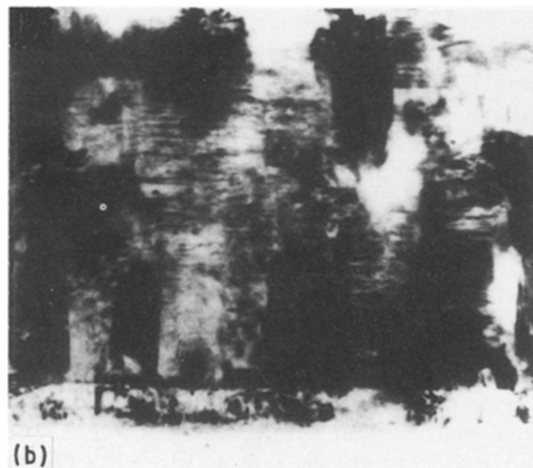

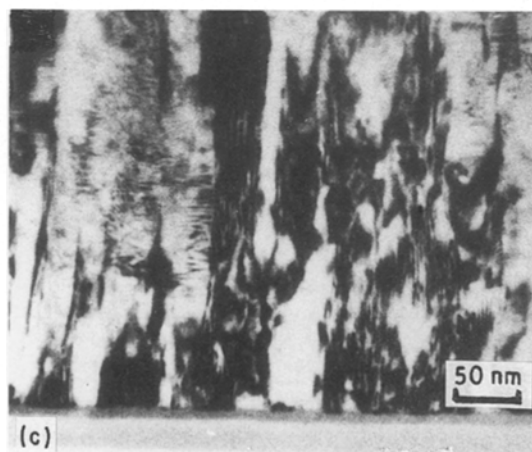

Figure 18 Cross-sectional TEM images of Co–Cr films deposited on (a) polyimide substrate, (b) Ti underlayer, and (c) Ge underlayer [151].

recording densities up to $D_{50} = 90.6$ kilo flux changes per cm. More recently, Schrauwen *et al.* [152] reconfirmed the advantage of using the amorphous Ge underlayer-PET substrate to promote the *c*-axis orientation of the Co–Cr films, provided the thickness of the Ge layer exceeds a critical value of about 200 nm. This is because thinner Ge underlayers will not seal the PET substrates completely.

The mechanism that promotes the nucleation of the *c*-axis orientation of the Co–Cr grains by amorphous Ge underlayers is not precisely known. Futamoto *et al.* [151] speculated that microareas having (1 1 0) and (1 1 1) atomic arrangements in the amorphous Ge underlayer might exist. They further reasoned that these atomic configurations are energetically stable and form hexagonal-like networks that match the (0 0 0 1) basal plane of the h c p Co–Cr lattice with only 2% deviation in the interatomic distance between Ge and Co–Cr. The microareas can then trigger the nucleation of the Co–Cr grains with the *c*-axis orientation. No evidence was given for such a mechanism.

For double-layer perpendicular recording media, Uesaka *et al.* [153] demonstrated an epitaxial growth relationship between the soft ferromagnetic Ni–Fe underlayer and the mildly hard Co–Cr layer. Developing a (1 1 1) texture in the f c c Ni–Fe underlayer is therefore beneficial in promoting the formation of the *c*-axis orientation of the Co–Cr films. Jhingan *et al.* [150] found that the (1 1 1) texture of the Ni–Fe underlayer is improved by reducing the oxygen content of the sputtering gas and increasing film thickness. The decrease in $\Delta\theta_{50}$ with an increase in film thickness is attributed to the preferential growth of the (1 1 1) direction and to the recrystallization of the Ni–Fe grains in the later stage of the film growth of the underlayer.

The microstructure of films prepared by either the sputtering or the evaporation process is almost always associated with internal stresses. Rarely are films free from residual stresses, and this occurs only when the gas pressure and substrate temperature are at critical values. The internal stress, σ_0, is generally resolved into two components: thermally-induced, σ_{th}, and intrinsic, σ_{in}, which account for all other temperature-independent mechanisms. σ_{th} is readily calculated from the thermal expansion coefficient difference, $\Delta\alpha$, and the temperature deviation, ΔT, between the deposit and the substrate. σ_{in} is not calculable unless the exact intrinsic mechanism is known. Following Aboaf [154], we have

$$\begin{aligned}\sigma_0 &= \sigma_{th} + \sigma_{in}\\ &= (\alpha_{subs.} + \alpha_{film})[E_{film}/(1 - \gamma_{film})]\,\Delta T + \sigma_{in}\end{aligned}$$

where E is Young's modulus and γ is Poisson's ratio. The presence of internal stresses in the Co–Cr films may adversely affect the magnetic and mechanical properties significantly. σ_0 could change the structural-sensitive magnetic properties, such as coercivity, substantially. It may also cause curling if the substrate is not rigid; it may even induce cracking.

For sputter-deposited films, the type of internal stresses changes from tensile to compressive with decreasing argon pressure or increasing substrate bias voltage [155]. The effect of ion bombardment during evaporation-deposition of Co–Cr was studied by Honda and Storer [128] and by Awano and Sato [119]. Both studies used the *e*-beam evaporation process coupled with ion bombardment. In the experiments of Honda and Storer, internal stress changes to compressive from tensile by the peening effect of ion bombardment. Awano and Sato estimated that the average energy imparted to Co and Cr atoms by argon ion bombardment was 17 eV at the point where the internal stress turned compressive from tensile. This energy is about a hundred times that imported during vacuum deposition. The observed changes in internal stresses are explained in terms of an increase in the amount of trapped argon in the Co–Cr films due to ion bombardment. It is seen in Fig. 19 that, as the amount of argon was increased from less than 0.03 at % in the absence of ion bombardment to 0.3 at %, the number of cracks was reduced (Fig. 19a and b). Further increase in the amount of trapped argon, to 0.8 at % and 1.2 at %, eliminated cracking altogether (Fig. 19c and d), even though internal stress still existed but was compressive. Also considered as further evidence of such explanation was the increase of the spacing of the (0 0 0 2) plane [119].

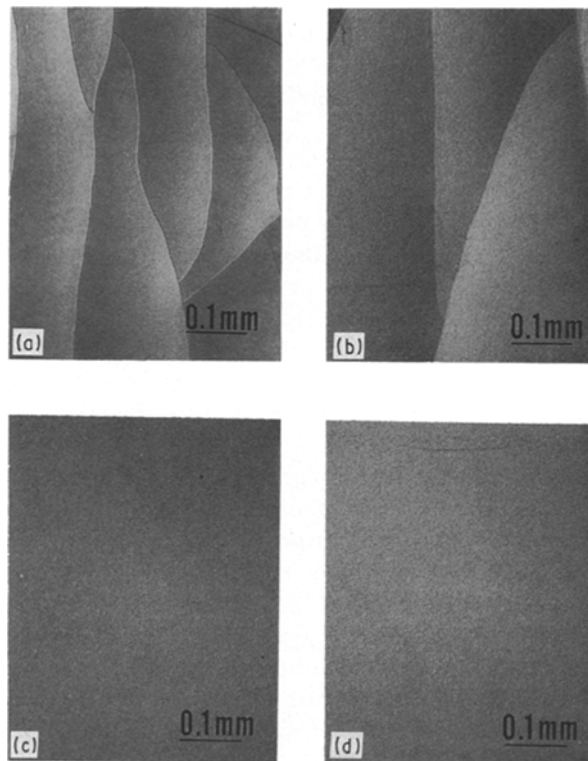

Figure 19 Cracks were first reduced and then disappeared as the amount of trapped argon was increased from (a) less than 0.03 at % without argon-ion bombardment to (b) 0.3 at %, (c) 0.8 at %, and (d) 1.2 at % [119].

References

1. M. H. KRYDER and A. B. BORTZ, *Phys. Today* **Dec** (1984) 20.
2. S.-I. IWASAKI and K. TAKEMURA, *IEEE Trans. Magn.* **MAG-11** (1975) 1173.
3. S.-I. IWASAKI and Y. NAKAMURA, *ibid.* **MAG-13** (1977) 1272.

4. A. H. ELTOUKHY, *J. Vac. Sci. Tech.* **A4** (1986) 539.
5. J. K. HOWARD, *ibid.* **A4** (1986) 1.
6. C. BONNEBAT, *IEEE Trans. Magn.* **MAG-23** (1987) 9.
7. CHIH-WEN CHEN, in "Magnetism and Metallurgy of Soft Magnetic Materials" (Dover Publications, New York, 1986).
8. T. CHEN and P. L. CAVALLOTTI, *Appl. Phys. Lett.* **41** (1982) 205.
9. M. SHIRAKI, Y. WAKII, T. TOKUSHIMA and H. TSUYA, *IEEE Trans. Magn.* **MAG-21** (1985) 1465.
10. W. ANDRA, H. DANAN and U. ROPKE, *ibid.* **MAG-20** (1984) 102.
11. C. KOOY and U. ENZ, *Philips Res. Rep.* **15** (1960) 7.
12. J. KACZER, *J. Appl. Phys.* **29** (1958) 569.
13. S. HONDA, T. YAMAKAWA and T. KUSUDA, *IEEE Trans. Magn.* **MAG-21** (1985) 1468.
14. V. M. FEDOSYUK, L. F. ILYUSHENKO, M. U. SHELEG and A. V. BOLTUSHKIN, *Thin Solid Films* **158** (1988) 7.
15. R. F. SOOHOO, *J. Appl. Phys.* **55** (1984) 2211.
16. J. S. NELSON, C. Y. FONG and I. P. BATRA, *ibid.* **63** (1988) 3049.
17. S.-I. IWASAKI, *IEEE Trans. Magn.* **MAG-16** (1980) 71.
18. *Ibid. Recent Magn. Electron.* **10** (1983) 101.
19. R. I. POTTER and I. A. BEARDSLEY, *IEEE Trans. Magn.* **MAG-16** (1980) 967.
20. I. B. ORTENBURGER and R. I. POTTER, *J. Appl. Phys.* **50** (1979) 2393.
21. I. S. BEARDSLEY, *ibid.* **53** (1982) 2582.
22. T. R. KOEHLER, *ibid.* **55** (1984) 2214.
23. P. SILVESTER and M. V. K. CHARI, *IEEE Trans. Power App. Syst.* **PAS-89** (1970) 1642.
24. T. SUZUKI and S.-I. IWASAKI, *IEEE Trans. Magn.* **MAG-18** (1982) 769.
25. I. A. BEARDSLEY and C. TSANG, *J. Appl. Phys.* **55** (1984) 2208.
26. Y. NAKAMURA, S. YAMAMOTO and S.-I. IWASAKI, *IEEE Trans. Magn.* **MAG-22** (1986) 376.
27. J. HOKKYO, I. SAITO and S. SATAKE, *ibid.* **MAG-16** (1980) 887.
28. H. N. BERTRAM, *ibid.* **MAG-21** (1985) 1397.
29. N. H. YEH, *ibid.* **MAG-21** (1985) 1338.
30. K. SHINAGAWA, H. FUJIWARA, F. KUGIYA, T. OKUWAKI and M. KUDO, *J. Appl. Phys.* **53** (1982) 2585.
31. S.-I. IWASAKI, Y. NAKAMURA and K. OUCHI, *IEEE Trans. Magn.* **MAG-15** (1980) 1456.
32. V. B. MINUHIN, *ibid.* **MAG-22** (1986) 388.
33. J.-G. ZHU and H. N. BERTRAM, *ibid.* **MAG-22** (1986) 379.
34. K. FUKUDA, Y. KITAHARA, F. MARUTA and J. EZAKI, *ibid.* **MAG-18** (1982) 1116.
35. C. W. CHEN and C. S. ALFORD, *J. Vac. Sci. Tech.* **A6** (1988) 128.
36. S. I. IWASAKI and K. OUCHI, *IEEE Trans. Magn.* **MAG-14** (1978) 849.
37. J. W. SMITS and F. J. A. DEN BROEDER, *Thin Solid Films* **127** (1985) 1.
38. H. TAMAI, K. TAGAMI and H. HAYASHIDA, *IEEE Trans. Magn.* **MAG-24** (1988) 2347.
39. J. C. ALLAN and R. D. FISHER, *ibid.* **MAG-23** (1987) 122.
40. T. YAMADA, N. TANI, M. ISHIKAWA, Y. OTA, K. NAKAMURA and A. ITOH, *ibid.* **MAG-21** (1985) 1429.
41. K. KOBAYASHI and G. ISHIDA, *J. Appl. Phys.* **52** (1981) 2453.
42. J. TADA, M. AKIHIRO, K. TAKEI, T. SATOH and T. SUZUKI, *IEEE Trans. Magn.* **MAG-22** (1986) 343.
43. T. SUZUKI and N. YOSHIDA, *J. Appl. Phys.* **63** (1989) 2929.
44. H. AWANO and H. MASUYA, *IEEE Trans. Magn.* **MAG-23** (1987) 2067.
45. K. INOUE, M. YOSHIKIYO and S. YOSHII, *ibid.* **MAG-23** (1987) 3651.
46. S.-I. IWASAKI, K. OUCHI and N. HONDA, *ibid.* **MAG-16** (1980) 1111.
47. J. A. THOMPSON and D. A. STEVENSON, *J. Appl. Phys.* **61** (1987) 3155.
48. P. E. CARCIA, *ibid.* **63** (1988) 5066.
49. M. OHKOSHI, K. TAMARI, S. HONDA and T. KUSUDA, *IEEE Trans. Magn.* **MAG-20** (1984) 788.
50. F. KUGIYA, M. SUZUKI, F. KANNO, Y. YOSHIDA, O. KITAKAMI, H. FUJIWARA and D. E. SPELIOTIS, *ibid.* **MAG-24** (1988) 2908.
51. J. DESSERRE and D. JEANNIOT, *ibid* **MAG-19** (1983) 1647.
52. P. BERNSTEIN and F. RIO, *ibid.* **MAG-23** (1987) 143.
53. T. MIZOGUCHI, N. AKUTSU and M. AKIMITSU, *J. Appl. Phys.* **61** (1987) 3158.
54. N. AKUTSU, M. AKIMITSU and T. MIZOGUCHI, *IEEE Trans. Magn.* **MAG-22** (1986) 1170.
55. A. MORISAKO, M. MATSUMOTO and M. NAOE, *ibid.* **MAG-22** (1986) 1146.
56. C. W. CHEN and C. S. ALFORD, *Lawrence Livermore National Laboratory Report UCID-20601* (1985).
57. J. W. SMITS, S. B. LUITJENS, F. J. A. DEN BROEDER and A. G. DIRKS, *J. Magn. Magn. Mat.* **31–34** (1983) 920.
58. J. A. THOMPSON and P. B. MEE, *IEEE Trans. Magn.* **MAG-20** (1984) 785.
59. T. M. COUGHLIN, J. H. JUDY and E. R. WUORI, *ibid.* **MAG-17** (1981) 3169.
60. T. WIELINGA and J. C. LODDER, *ibid.* **MAG-17** (1981) 3178.
61. J. C. LODDER, T. WIELINGA and J. WORST, *Thin Solid Films* **101** (1983) 61.
62. H. MAEDA, *J. Appl. Phys.* **54** (1983) 2429.
63. J. A. THORNTON, in "Deposition Technologies for Films and Coating," edited by R. F. Bunshah (Noyes Publications, New York, 1982).
64. S. KADOKURA, T. TOMIE and M. NAOE, *IEEE Trans. Magn.* **MAG-17** (1981) 3175.
65. K. ROLL, R. KUKLA, M. MAYR and W. D. MUNZ, *ibid.* **MAG-20** (1984) 63.
66. S.-I. IWASAKI, K. OUCHI, K. SAIKI and M. KIMURA, *ibid.* **MAG-22** (1986) 1158.
67. D. RAVIPATI, J. M. SIVERTSEN and J. H. JUDY, *ibid.* **MAG-22** (1986) 1152.
68. M. KUME, D. KISHIMOTO, Y. NAKATSUKA and Y. ABE, *ibid.* **MAG-22** (1986) 1161.
69. M. MAYR, K. KASTNER, R. KUKLA and R. LUDWIG, *ibid.* **MAG-23** (1987) 131.
70. Y. NIIMURA, S. NAKAGAWA and M. NAOE, *ibid.* **MAG-23** (1987) 2043.
71. T. M. COUGHLIN, E. R. WUORI and J. H. JUDY, *J. Vac. Sci. Tech.* **20** (1982) 171.
72. R. KUKLA, J. KIESER and M. MAYR, *IEEE Trans. Magn.* **MAG-23** (1987) 137.
73. M. OHKOSHI and T. KUSUDA, *J. Vac. Sci. Tech.* **A5** (1987) 2859.
74. Y. SUZUKI, K. TAKIGUCHI, M. YOSHITAKE, T. YOTSUYA and S. OGAWA, *ibid.* **A5** (1987) 1870.
75. J. A. THOMPSON and D. A. STEVENSON, *IEEE Trans. Magn.* **MAG-21** (1985) 1441.
76. Y. NAKATSUKA, H. TANAKA, T. KYOZUMI and Y. ABE, *ibid.* **MAG-22** (1986) 1002.
77. N. HONDA and H. UCHIYAMA, *ibid.* **MAG-23** (1987) 3657.
78. H. R. KAUFMANN, *J. Vac. Sci. Tech.* **15** (1978) 272.
79. H. S. GILL and M. P. ROSENBLUM, *IEEE Trans. Magn.* **MAG-19** (1983) 1044.
80. W. T. MALONEY and C. D. LUSTIG, *ibid.* **MAG-20** (1984) 521.
81. R. D. FISHER, V. S. AU-YEUNG and B. B. SABO, *ibid.* **MAG-20** (1984) 806.
82. S. KADOKURA and M. NAOE, *ibid.* **MAG-18** (1982) 1113.
83. R. LUDWIG, K. KASTNER, R. KUKLA and M. MAYR, in "Digest of International Conf. on Magnetic Recording Media CMD2" (1986).
84. K. NAKAMURA, T. YAMADA, Y. OHTA and A. ITOH, *IEEE Trans. Magn.* **MAG-18** (1982) 1080.
85. M. OHKOSHI, R. OHKATA, K. INOUE, S. HONDA and T. KUSUDA, *Jpn. J. Appl. Phys.* **19** (1980) 1807.
86. E. KRIKORIAN and R. J. SNEED, *J. Appl. Phys.* **37** (1966) 3674.
87. H. MAEDA, *ibid.* **54** (1983) 2429.

88. T. CHEN, G. B. CHARLAN and T. YAMASHITA, *ibid.* **54** (1983) 5103.
89. D. W. HOFFMAN and J. A. THORNTON, *J. Vac. Sci. Tech.* **17** (1980) 380.
90. S. KIM, D. J. HENDERSON and P. CHANDHARI, *Thin Solid Films* **47** (1977) 155.
91. A. FEUERSTEIN and M. MAYR, *IEEE Trans. Magn.* **MAG-20** (1984) 51.
92. R. SUGITA, T. KUNIEDA and F. KOBAYASHI, *ibid.* **MAG-17** (1981) 3172.
93. R. SUGITA and K. KOBAYASHI, *ibid.* **MAG-18** (1982) 1818.
94. R. SUGITA, *ibid.* **MAG-20** (1984) 687.
95. R. SUGITA, T. NAMBU and T. SAKAMOTO, *ibid.* **MAG-23** (1987) 2449.
96. K. HONDA, H. SUGITA and Y. SAKAMOTO, *ibid.* **MAG-23** (1987) 2040.
97. K. YOSHIDA, K. IMAGAWA, Y. HONDA, M. FUTOMOTO and H. DAIMON, *Jpn. J. Appl. Phys.* **27** (1988) 1240.
98. C. F. BRUCKER, M. M. ROMACH and W. E. YETTER, *IEEE Trans. Magn.* **MAG-24** (1988) 2359.
99. S. HONDA and J. STORER, *ibid.* **MAG-22** (1986) 337.
100. F. A. PRONK and J. C. LODDER, *ibid.* **MAG-24** (1988) 1744.
101. T. OSAKA, N. KASAI, I. KOIWA, F. GOTO and Y. SUGANUMA, *J. Electrochem. Soc.* **130** (1983) 568.
102. T. OSAKA, I. KOIWA, M. TODA, T. SAKUMA, Y. YAMAZAKI, T. NAMIKAWA and F. GOTO, *IEEE Trans. Magn.* **MAG-22** (1986) 1149.
103. I. KOIWA, H. MATSUBARA, T. OSAKA, Y. YAMAZAKI and T. NAMIKAWA, *J. Electrochem. Soc.* **133** (1986) 667.
104. I. KOIWA, Y. OKABE, H. MATSUBARA, T. OSAKA and F. GOTO, *J. Magn. Soc. Jpn.* **58** (1985) 414.
105. K. ITO, O. TAKANO and H. MATSUDA, in Asst. 66th Conference of the Metal Finish Society, Japan, 1980, p. 8.
106. T. CHEN and P. L. CAVALLOTTI, *IEEE Trans. Magn.* **MAG-18** (1982) 1125.
107. H. HOFFMANN, L. KOCHANOWSKY, H. MANDL, K. KASTNER, M. MAYR, W. D. MUNZ and K. ROLL, *ibid.* **MAG-21** (1985) 1432.
108. S. KAWAI and R. UEDA, *J. Electrochem. Soc.* **122** (1975) 32.
109. N. TSUYA, T. TOKUSHIMA, M. SHIRAKI, Y. WAKUI, T. SAITO, H. NAKAMURA, S. HAYANO, A. FURUGORI and M. TANAKA, *IEEE Trans. Magn.* **MAG-22** (1986) 1140.
110. N. TSUYA, T. TOKUSHIMA, M. SHIRAKI, Y. WAKUI, Y. SAITO, H. NAKAMURA and Y. KATSUMATA, *ibid.* **MAG-23** (1987) 53.
111. N. TSUYA, T. TOKUSHIMA, M. SHIRAKI and Y. UMEHARA, *ibid.* **MAG-24** (1988) 1790.
112. M. OHKOSHI, S. ODA and T. KUSUDA, *ibid.* **MAG-23** (1987) 2248.
113. C. ALLIBERT, C. BERNARD, N. VALIGNAT and M. DOMBRE, *J. Less Common Metals* **59** (1978) 211.
114. W. G. MOFFATT, in "The Handbook of Binary Phase Diagrams," Vol. 2 (General Electric Co., Schenectady, 1981).
115. J. W. SMITS, S. B. LUITJENS and F. J. A. DEN BROEDER, *J. Appl. Phys.* **55** (1984) 2260.
116. M. HANSEN, in "Constitution of Binary Alloys" (McGraw-Hill Book Co., New York, 1958) p. 467.
117. "Metals Handbook" Vol. 8, 8th Edn edited by T. Lyman (American Society for Metals, Metals Park, 1973) p. 287.
118. Y. MATSUNAGA, *Kinzoku-No-Kenkyu* **8** (1931) 549.
119. H. AWANO and T. SATO, *Jpn. J. Appl. Phys.* **27** (1988) L880.
120. H. MASUYA and H. AWANO, *IEEE Trans. Magn.* **MAG-23** (1987) 2064.
121. R. D. FISHER, V. S. AU-YEUNG and B. B. SABO, *ibid.* **MAG-20** (1984) 806.
122. P. J. GRUNDY and M. ALI, *J. Magn. Mater.* **40** (1983) 154.
123. T. MARO, O. KITAKAMI, and H. FUJIWARA, *Jpn. J. Appl. Phys.* **27** (1988) L687.
124. Y. MAEDA and M. ASAHI, *IEEE Trans. Magn.* **MAG-23** (1987) 2061.
125. Y. MAEDA and M. TAKAHASHI, *Jpn. J. Appl. Phys.* **28** (1989) L-248.
126. W. ANDRA and H. DANAN, *IEEE Trans. Magn.* **MAG-23** (1987) 62.
127. J.-W. LEE, B. G. DEMCZYK, K. R. MOUNTFIELD and D. E. LAUGHLIN, *ibid.* **MAG-23** (1987) 2455.
128. S. HONDA and J. STORER, *ibid.* **MAG-22** (1986) 337.
129. T. KUSUDA, S. HONDA and M. OHKOSHI, *J. Appl. Phys.* **53** (1982) 2338.
130. S. YASUGI, S. HONDA, M. OHKOSHI and T. KASUDA, *ibid.* **52** (1981) 2298.
131. J.-W. LEE, B. G. DEMCZYK, K. R. MOUNTFIELD and D. E. LAUGHLIN, *ibid.* **61** (1987) 3813.
132. R. J. ARTLEY, K. OUCHI and S.-I. IWASAKI, *IEEE Trans. Magn.* **MAG-24** (1988) 2335.
133. D. A. GLOCKER, W. E. YETTER and J.-S. GAU, *ibid.* **MAG-22** (1986) 331.
134. S. YOICHI, H. KAZUYOSHI, N. TARO, S. RYUJI and T. MIHO, *ibid.* **MAG-23** (1987) 3654.
135. T. SPALVINS and W. A. BRAINARD, *J. Vac. Sci. Tech.* **11** (1974) 1186.
136. T. SPALVINS, *Thin Solid Films* **64** (1979) 143.
137. J. W. PATTERN, *ibid.* **63** (1979) 121.
138. K. H. GUENTHER, *Appl. Optics* **20** (1981) 1034.
139. R. SUGITA, *IEEE Trans. Magn.* **MAG-20** (1984) 687.
140. J. W. NIEUWENTHUIZEN and H. B. HAASTRA, *Philips Tech. Rev.* **27** (1966) 87.
141. A. G. DIRKS and H. J. LEAMY, *Thin Solid Films* **47** (1977) 219.
142. E. M. SIMPSON and J. H. JUDY, *IEEE Trans. Magn.* **MAG-22** (1986) 1167.
143. M. MATSUOKA, Y. HOSHINO, M. NAOE and S. YAMANAKA, in Proceedings of the Conference IECE Japan S15-6 (1983) p. 254.
144. Y. TANAKA, H. ITO, T. SONODA and R. NISHIKAWA, *IEEE Trans. Magn.* **MAG-23** (1987) 2046.
145. A. VAN DER DRIFT, *Philips Res. Rep.* **22** (1967) 267.
146. Y. NIIMURA, S. NAKAGAWA and M. NAOE, *IEEE Trans. Magn.* **MAG-22** (1986) 1164.
147. H. S. GILL and M. P. ROSENBLUM, *ibid.* **MAG-19** (1983) 1644.
148. H. S. GILL and T. YAMASHITA, *ibid.* **MAG-20** (1984) 776.
149. T. TOMIE, M. OGUSAWARA, Y. KATO and I. OUCHI, *Jpn. J. Appl. Phys.* **27** (1988) 1890.
150. A. K. JHINGAN, R. R. DUBIN and L. F. HERTE, *IEEE Trans. Magn.* **MAG-20** (1984) 779.
151. M. FUTAMOTO, Y. HONDA, H. KAKIBAYASHI and K. YOSHIDA, *ibid.* **MAG-21** (1985) 1426.
152. C. P. G. SCHRAUWEN, J. P. C. BERNARDS, R. W. DE BIE, G. J. P. VAN ENGELEN, H. H. STEL, V. ZIEREN and S. B. LUITJENS, *ibid.* **MAG-24** (1988) 1901.
153. Y. UESAKA, S. HISHIYAMA and H. FUZIWARA, in Proceedings of the 1982 Sendai Symposium, Tokoku University, Japan, 1982.
154. J. A. ABOAF, *J. Electrochem. Soc.* **116** (1969) 1736.
155. D. W. HOFFMAN and J. A. THORNTON, *Thin Solid Films* **40** (1977) 355.

Received and accepted 30 April 1990